Pacific Northwest
NATIONAL LABORATORY

PNNL-33346
AAX-RPT-001

Characterization of Contaminants and Mobility in WMA A-AX Boreholes D0006 and D0008

August 2022

JE Szecsody
HP Emerson
RD Mackley
MM Snyder
CT Resch
SR Baum

U.S. DEPARTMENT OF ENERGY

Prepared for the U.S. Department of Energy
under Contract DE-AC05-76RL01830

DISCLAIMER

PACIFIC NORTHWEST NATIONAL LABORATORY
operated by
BATTELLE
for the
UNITED STATES DEPARTMENT OF ENERGY
under Contract DE-AC05-76RL01830

Printed in the United States of America

Available to DOE and DOE contractors from the Office of Scientific and Technical Information,
P.O. Box 62, Oak Ridge, TN 37831-0062
www.osti.gov
ph: (865) 576-8401
fax: (865) 576-5728
email: reports@osti.gov

Available to the public from the National Technical Information Service
5301 Shawnee Rd., Alexandria, VA 22312
ph: (800) 553-NTIS (6847)
or (703) 605-6000
email: info@ntis.gov
Online ordering: http://www.ntis.gov

PNNL-33346
AAX-RPT-001

Characterization of Contaminants and Mobility in WMA A-AX Boreholes D0006 and D0008

August 2022

JE Szecsody
HP Emerson
RD Mackley
MM Snyder
CT Resch
SR Baum

Prepared for
the U.S. Department of Energy
under Contract DE-AC05-76RL01830

Pacific Northwest National Laboratory
Richland, Washington 99354

Summary

This study was initiated to determine if subsurface contaminants in the A-AX vadose zone at the Hanford site (boreholes D0006 and D0008) caused corrosion of nearby stainless steel well casings (299-E-24-19, 299-E25-46, and 299-E25-236) and, based on the type and distribution of contaminants, determine if contaminants are from one or more sources including a) the A-104 and/or A-105 tanks, b) the 242A evaporator, and c) the 200-E-286 ditch. A tiered approach was used for characterizing contaminants in vadose zone sediments starting with mobile and total contaminant concentrations (Tier 1), characterizing contaminant speciation (Tier 2), and measuring contaminant leaching (Tier 3). Total and mobile contaminant measurements at seven depths showed elevated sulfate and nitrate in all samples (130 to 280 ft depth), elevated chloride in five depths, and no elevated radionuclides except I-129 in D0006 at 206 to 208 ft depth. If these contaminants were initially acidic, stainless-steel corrosion would occur. However, because sediments likely have a high acid neutralization capacity, an acidic spill would have been neutralized within tens of feet, so casing corrosion would likely occur in shallow sediments. GEL labs data also shows low (but above natural) chromate from shallow to 170 ft depth, then higher chromate to 280 ft, suggesting a surface Cr spill or casing corrosion. GEL labs data also showed evidence of more than one plume, with deep nitrate, sulfate, and chloride migration, but only shallow tritium migration. Tritium should migrate nearly unretarded in the subsurface like nitrate and chloride. Elevated aqueous cations and anions in the D0006 206 to 208' depth pore water (SO_4^{2-}, NO_3^-, Na^+, K^+, Ca^{2+}, Mg^{2+}, Si) could be the result of acid disposal and calcite dissolution at shallow depth, with deeper migration of SO_4^{2-}, NO_3^- from acids and Ca^{2+} and $Mg^{2+}$from calcite. Elevated Si (160 mg/L) indicates dissolution of clays or other silicates, which can also occur in acids. Acid extractable metals did show elevated Cr (but not Fe, Ni, Mo, and Mn) above natural levels, which may indicate stainless-steel well corrosion or transport of metals from a shallow spill.

The elevated I-129 in D0006 at 206 to 208' depth was low with 0.34 μg/g in pore water and 1.5 μg/g total extractable I-129 in the sediment, which indicates significant fraction of I-129 was bound in one or more precipitates. Although total I-129 was below detection limits in most extractions due to high molybdate interference, I-127 analysis provided some insight into potential precipitate phases. Total I-127 was mainly extracted by acetate or acetic acid (67%), which may be iodine in calcite. Inorganic carbon measurement identified 1.65% calcite, and total organic carbon (TOC) was below detection limits, so iodine was not associated with organic matter. Nearly all the I-127 was present as iodide. In 1-D leach experiments, I-127 as iodide leached from the sediment within 2 pore volumes. Due to high and dynamic molybdate leaching from the sediment and interference with I-129 analysis, there were few quantifiable I-129 measurements. The calculated molybdate release rates from the sediment suggested Mo was being released from the same precipitate phase, such as molybdate incorporated into calcite.

Overall, because there was little radioactive contamination measured in D0006 and D0008 boreholes, potential releases from A-104 and A-105 did not reach this location south of the A tank farm. Elevated cations and anions found in D0006 and D0008 at depth as the result of acidic disposal could cause shallow stainless steel casing corrosion. The nearby 242A evaporator generally contained alkaline waste and tritium, but the nearby 200-E-286 ditch generally contained high Cl^- liquid effluent, so these are unlikely to be acidic sources.

Acknowledgments

This work was funded by Cindy Tabor at Washington River Protection Solutions, LLC (WRPS) under a contract. Many thanks to Sarah Springer at Central Plateau Cleanup Company (CP Co) for supplying additional HEIS data used for comparison to results in this study. Additional thanks to Marcel Bergeron, Sunil Mehta, Kim Schuyler, Jacob Reynolds, Doug Hildebrand, Chris Cearlock, and others for thoughtful comments on the interpretation of the data.

Acronyms and Abbreviations

APW	artificial porewater
CCu	Cold Creek Unit
DI	deionized water
H1	Hanford formation 1
H2	Hanford formation 2
HEIS	Hanford Environmental Information System
IC	ion chromatograph
ICP-MS	inductively coupled plasma-mass spectrometry
ICP-OES	inductively coupled plasma-optical emission spectrometry
KPA	kinetic phosphorescence analysis
LSC	liquid scintillation counting
MDL	minimum detectable level
ND	non-detect
NDIR	non-dispersive infrared
NQAP	Nuclear Quality Assurance Program
PNNL	Pacific Northwest National Laboratory
PTFE	polytetrafluoroethylene
PVDF	polyvinylidene fluoride
sequential extractions	a series of six liquids of increasing acidity used to measure the range of contaminants in different surface phases sediments from highly mobile (aqueous) to highly immobile in low solubility precipitates
SpC	specific conductivity
TC	total carbon
TIC	total inorganic carbon
TMAH	tetramethylammonium hydroxide - an alkaline solution used to extract iodine from sediments
TOC	total organic carbon
UV	ultraviolet

Contents

Figures

Tables

1.0 Introduction

The objective of this study in the A-AX tank area was to identify tank waste constituents in sediments and pore water, sediment phases that may be altered by contact with tank wastes and estimate chemical and physical properties of the vadose zone sediments that influence contaminant movement (Tabor and Schuyler, 2020, RPP-PLAN-63020, Rev 1, Special Study, p B-1, defined in detail in research questions below).

The following research questions were considered:

1. What are the chemical and physical properties of the vadose zone soil that can influence contaminant movement in the subsurface? (principle study question, PSQ, #2 Klages et al., 2021)
2. What natural components of the vadose zone could be altered by contact with tank waste solutions? (PSQ #4)
3. Are there tank waste constituents still detectable in the vadose zone after the bulk of the waste has passed through the area? (PSQ #4)
4. What is the concentration and distribution between aqueous and sediment phases of naturally occurring vadose zone and tank waste constituents? (PSQ #4)
5. How can this data inform the conceptual site model for contaminant transport and potential for well corrosion amid impacts from acidic waste releases? (from Tabor and Schuyler, 2020).

The interest in identification of anthropogenic contaminants in A-AX vadose zone sediments is that some contaminants could have caused stainless steel well corrosion, show evidence of well corrosion, or identify the source(s) of the contamination, as described in the sampling and analysis plan (Tabor and Schuyler, 2020, RPP-PLAN-63020, Rev 1) and data quality objectives (RPP-RPT-60227 and Tabor, 2021). Multiple wells were previously decommissioned due to corrosion, included 299-E-24-19, 299-E25-46, and 299-E25-236. Potential contamination sources include A-104 and A-105 tanks, 242A evaporator, and the 200-E-286 ditch. For this study, two boreholes (D0006 and D0008) were drilled south of the A-tank farm to collect sediments to help identify nearby potential contaminant sources (Figure 1).

A tiered approach was used for characterizing contaminant concentrations and potential for migration in samples from boreholes D0006 and D0008, as well as physical properties of the vadose zone sediments that can influence contaminant movement, as described in Appendix B of the Sampling and Analysis Plan (Tabor and Schuyler, 2020, RPP-PLAN-63020, Rev 0). The analyses conducted in this tiered approach includes:

- **Tier 1:** Estimate mobile and total contaminant concentrations and sediment physical properties that influence contaminant movement
- **Tier 2:** Characterize contaminant speciation as an indicator of contaminant movement potential
- **Tier 3:** Measure contaminant leaching mass and release rate from sediments under relevant conditions

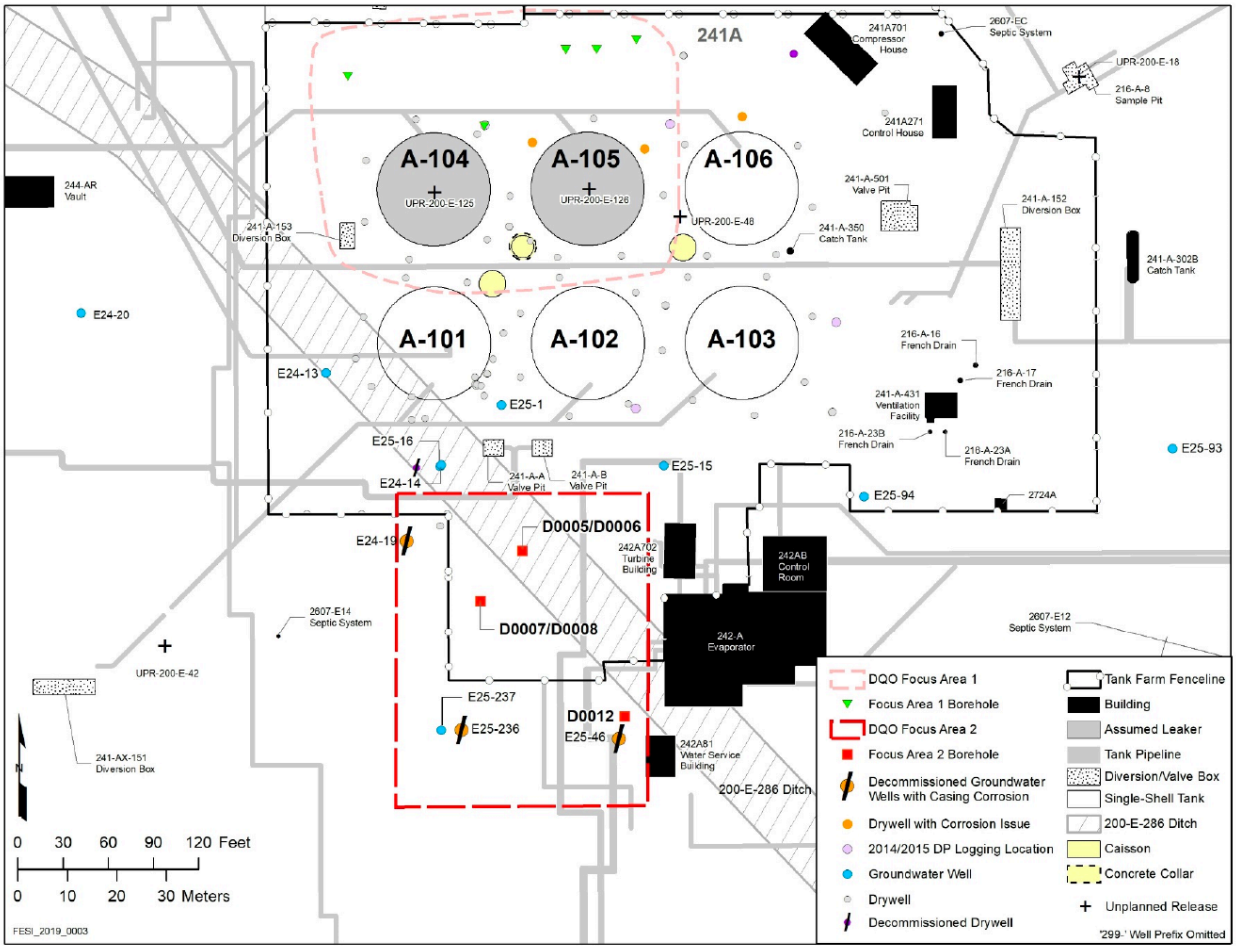

Figure 1. Study area location south of the A-AX tank farm (from Tabor and Schuyler, 2020).

For Tier 1, mobile contaminant concentrations are measured with a water extraction of the field sediment with subsequent analysis of contaminants in the extracted water. The total contaminant concentrations are characterized with an acid extraction for most contaminants in the sediment (alkaline extraction for I-129) and analysis of the total contaminant concentration in the extracted liquid (described in detail in the analysis section). Additional geochemical parameters that may influence contaminant movement are measured in the water extraction and include pH, specific conductivity, total inorganic and organic carbon (TIC and TOC, respectively), alkalinity, and selected anions. Sediment physical properties measured and include sediment grain size distribution, sediment moisture content, and sediment bulk density. Constituents being analyzed in Tier 1 include the following contaminants of concern (COCs): total U, U(VI), Tc-99, Cs-137, Sr-90, total iodine-127/129, and selected aqueous indicator anions: Cl, F, SO_4, NO_3. Total U and hexavalent U (U(VI)) will both be measured to consider the redox conditions as U mobility is profoundly impacted by its oxidation state. Although I-127 is naturally occurring and non-radioactive, it will be measured alongside I-129 to inform potential behavior of I-129 and because potential remediation technologies are not isotope-specific. Based on Tier 1 results, additional Tier 2 geochemical analyses may be conducted for selected contaminants at levels that are greater than natural background or detection limits for isotopes that are not naturally occurring (i.e., not all contaminants measured in Tier 1 experiments are measured in Tier 2 and Tier 3 experiments). These data will help inform on the location of major COCs and describe the sediment characteristics. They will be compared with previous characterization studies to understand potential sources of contamination and sediment alterations that may have occurred upon interaction with wastes.

For Tier 2, with samples and contaminants prioritized based on Tier 1 analysis, the mobility of selected contaminant species in field-contaminated sediments is characterized using different liquid extractions that include: a) six sequential liquid extractions, b) 1000-h carbonate extraction, and c) tetramethylammonium hydroxide (TMAH) extraction. The sequential extractions consist of a series of progressively more acidic liquids that remove a wide range of contaminants in aqueous, adsorbed, and different precipitate phases. The 1000-h carbonate extraction dissolves calcite, which may contain some contaminants including uranium and Sr-90. The TMAH extraction is used to dissolve precipitates and surface organics that contain iodine species. Water and acid extractions are also conducted with measurement of major cations and metals that may be associated with stainless steel corrosion (B, Cr, Cu, Fe, Mn, Mo, Ni, T, Ti, and V), and aqueous anions not previously analyzed in Tier 1. Based on Tier 2 results, selected contaminants that are present in significant concentrations and are potentially mobile are additionally characterized in Tier 3 experiments.

For Tier 3, leaching mass and rate of selected contaminants from the field sediments is measured in 1-D column leach experiments. These leach experiments include stop flow events so that the contaminant release rate from sediments can be characterized. In addition, five different iron/manganese extractions are conducted to characterize the ferrous and ferric phases in sediments. These redox couples are used to further define geochemical conditions that influence the mobility of contaminants. Experiments conducted in Tier 2 and 3 will inform on the long-term mobility of the contaminants that are present in the subsurface including the approximate rates of release from sediments.

2.0 Background

Corrosion of the stainless steel in wells and decommissioning of three wells (299-E-24-19, 299-E25-46, and 299-E25-236) south of A-AX may have been caused by leaks from Tanks A-104 and/or A-105, or from other leaks. Other potential sources that could cause well casing corrosion include a) discharges to the 200-E-286 ditch between 1946 and 1953 with high chloride effluent, and b) a 60,000-gallon leak from a ruptured water line southeast of 241-A-501 Valve Pit in 1978 (Tabor and Schuyler, 2020, RPP-PLAN-63020, Rev 1).

Stainless steel corrosion is the result of pitting of the passivation layer (i.e., Cr_2O_3) on the base metal surface (He et al. 2009, Marcus, 1998). Corrosion of both 316L and 304L stainless steels is higher at welds (Garcia et al., 2008, Martin et al., 2009) and in aqueous environments with high chloride, acid, sulfide, and carbonate content (Li et al., 2014; Robertson, 1991). A chloride concentration of 100 mg/L is the threshold above which stainless steel can pit or corrode (Sedricks 1996), although the pH also significantly affects the corrosion rate. Given the elements present in the stainless steel of the well casing (i.e., 316L is ~70% Fe, 16% Cr, 10% Ni, 2% Mo, ~1.1% Mn, and 0.4% Si, with trace concentrations of other elements), when the three wells were in use, elevated levels of Ni, Mn, Fe, and Cr were detected, which indicated casing corrosion. In addition, Tc-99 has exceeded the drinking water standard in 299-E-25-235 since 2012, which may have been associated with upgradient sources such as WMA C or the B-complex or possibly vadose zone pore water seeping through the A-AX corroded casing at a shallower depth but being measured in groundwater (at 295 ft or 90 m depth).

Hence, additional characterization was necessary for development of a conceptual model of the long-term mobility of contaminants for the regulatory decision-making process.

3.0 Experimental

3.1 Sediments

Sediment samples used in this study were taken from two small diameter cores (i.e., 1 inch diameter by 6 inch length) from boreholes D0008 and D0006. All samples were received in sealed core sleeves and were stored in a refrigerator at 4ºC until characterization was conducted. Experiments indicate whether bulk or sieved sediments were used for each analysis. Seven samples at specific depths were chosen for this study (Table 1), based on elevated anion concentrations measured in preliminary screening. Images of the sediment samples showed samples were predominantly sand or silt sized (Figure 2), which was quantified by particle size analysis (next section).

Table 1. Sediments analyzed in this study.

Borehole	Depth (ft)	HEIS #	Lithologic Unit
D0008A	264 - 266	B3TLF5	H2
D0008A	278 - 280	B3TLF9	CCu (silt)
D0008A	284 - 286	B3TLH3	CCu (gravel)
D0006	134 - 136	B3TF28	H1
D0006A	181 - 183	B3TF32	H2
D0006A	206 - 208	B3TF36	H2
D0006A	275 - 277	B3TF44	CCu (silt)

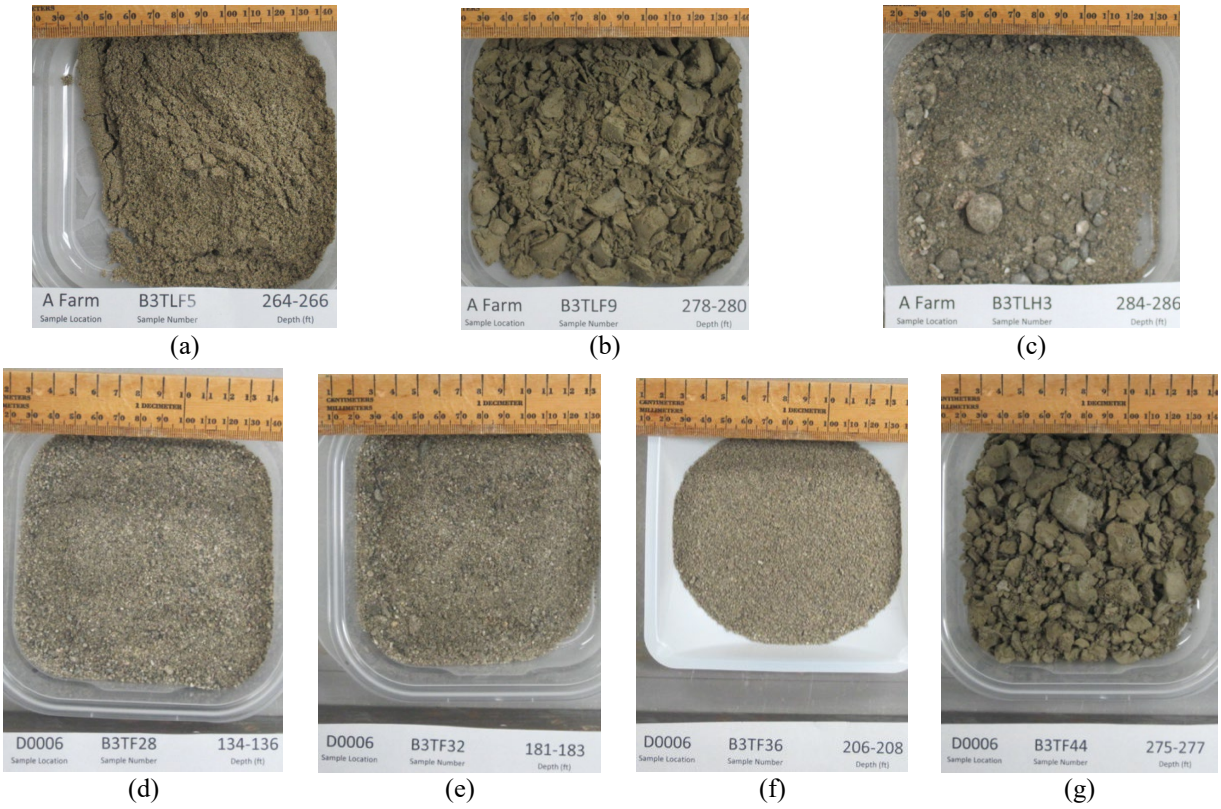

(a) (b) (c)

(d) (e) (f) (g)

Figure 2. Images of sediment samples from borehole D0008 (a - c) and D0006 (d - g).

3.2 Tier 1 Geochemical and Physical Characterization

In this study, the < 2 mm size fraction of the sediment was used for Tier 1, 2, and 3 chemical characterization and Tier 1 physical characterization (as defined in the current revision of the sampling and analysis plan, Section B2.2, Table B-2). For Tier 1 chemical analysis, a 1:1 sediment:deionized (DI) water extraction was conducted (EPA 9045D, Rhoades 1996), which consisted of mixing sediment and DI water in a sealed vial for 50 minutes by placing the tube on a slow (<30 rpm) rotary mixer or orbital shaker. The tube is then centrifuged at 3000 rpm for 10 minutes (or allowed to settle for 10 minutes), then liquid is drawn off the top of the sediment and filtered (0.45-μm nylon or polyvinylidene fluoride, PVDF) for analysis. This extraction is conducted at room temperature (20°C to 25°C). After filtering, the aqueous sample is stored at 4°C before analysis (Um et al., 2009, Zachara et al., 2007). The aqueous samples were analyzed for pH, aqueous specific conductance (SpC), aqueous contaminants (based on initial 'quick turn' analysis conducted by GEL laboratories, potentially including total U, U(VI), Tc-99, Cs-137, Sr-90, total iodine-127/129), and selected aqueous indicator anions (based on initial 'quick turn' analysis, potentially including: Cl, F, SO_4, and NO_3). The moisture content of the sediment was measured separately by weighing 3 to 30 g of moist sediment, drying for 48 h at 105 °C, and weighing the dry sediment. The moisture content is the mass of water (moist sediment minus dry sediment) divided by the dry sediment weight. Dry sediment was not used for further analyses.

An acid extraction (1:3 sediment:solution, Um et al., 2009, Zachara et al., 2007) was also conducted with the selected sediments. This extraction consisted of adding sediment and 8 M HNO_3 to the sample (at the 1:3 dry sediment/acid ratio) in a polytetrafluoroethylene (PTFE) tube, then heating the sample for 3 hours at 90°C. After 3 hours, the liquid samples were centrifuged, and liquid filtered (0.45-μm PTFE or PVDF). Analysis of the extracted solution included total U and U(VI), Tc-99, Cs-137, Sr-90, and total iodine-127/129 (analytical techniques are described in Section 3.5).

Physical characterization of the sediment samples included measurement of the particle size distribution, dry bulk density, and moisture content. The particle size distribution was quantified by laser particle size analysis (ASTM D4464) for the < 2 mm size fraction. The 0.5-, 1-, 2-, and 4-mm size fractions of the sediment were quantified by sieving (ASTM D6913). The dry bulk density was quantified using ASTM D7263, and moisture content by ASTM D2216. Dried sediment samples were also analyzed for total inorganic and organic carbon using a carbon analyzer (Section 3.5).

3.3 Tier 2 Geochemical Characterization

Tier 2 chemical characterization included: a) water extraction, b) acid extraction, c) 1000-hour carbonate extraction, d) tetramethylammonium hydroxide (TMAH) extraction, and e) six sequential liquid extractions. The water and acid extractions were the same as in Tier 1 (1:1 sediment:DI water), but chemical analysis was different and included alkalinity, selected contaminant speciation, major cations and metals that may be associated with stainless steel corrosion (Cr, Fe, Mn, Mo, Ni, and Si), and aqueous anions (Br^-, Cl-, F-, NO_3^-, NO_2^-, PO_4^{-3}, SO_4^{-2}, only for water extracts) not previously analyzed in Tier 1. The only radionuclide analyzed in Tier 2 was I-129 and associated I-127, so extractions were analyzed for total I-129, total I-127, I-129 species, and I-127 species (Section 3.5). The 1000-h carbonate extraction was used to extract contaminants (including iodine) in carbonate (Kohler et al., 2004). This extraction solution consists of 0.0144 mol/L $NaHCO_3$ and 0.0028 mol/L Na_2CO_3 at pH 9.3. The sediment is mixed with the solution in a batch reactor for 1000 hours. With this extraction solution, there is no net carbonate dissolution or precipitation, but metals precipitated in calcite are expected to equilibrate with the aqueous solution over the 1000 h reaction time due to continuous slow carbonate precipitation and dissolution. The tetraethylammonium hydroxide (TMAH) extraction was used to dissolve iodine precipitates (McNally 2011; Watts and Mitchell 2008). Previous research has demonstrated quantitative

removal of iodine from certified standard sediments with this TMAH extraction. For this extraction, 1 g of sediment was reacted with 20 mL of 5% TMAH (50-g/L solution) at 70°C for 3 h.

The sequential liquid extractions (Gleyzes et al. 2002, Beckett 1989, Larner et al. 2006, Sutherland and Tack 2002, Massop and Davison 2003) consisted of mixing sediment with increasingly acidic solutions at a 1:3 sediment:solution on the < 2 mm grain size fraction with measurement of selected contaminants (total I-129, total I-127, I-129 species, I-127 species as they were elevated in Tier 1). The sequential extractions were used to characterize the contaminant surface phases and consisted of: 1) artificial pore water (APW, Table 2) for 1 hour, 2) ion exchange solution (0.5 mol/L $Mg(NO_3)_2$ for 1 h), 3) weak acetate extraction (1 mol L^{-1} NaOAc, pH 5, 1 h), 4) acetic acid extraction (0.44 mol L^{-1} acetic acid, 0.1 mol L^{-1} $Ca(NO_3)_2$, pH 2.3, 5 days) (Kohler et al., 2004), 5) Fe oxide extraction (0.1 mol L^{-1} ammonium oxalate, 0.1 mol L^{-1} oxalic acid, 1 h) (Chao and Zhou, 1983), and 6) strong acid extraction (8 mol L^{-1} HNO_3, 95°C, 3 h). It should be noted that these extractions are operationally defined and may not be strictly representative of the targeted fractions due to the complexity of these systems. Extraction 1 targets aqueous iodine species, whereas extraction 2 targets exchangeable, adsorbed iodine species from the sediment. Extractions 3 through 6 operationally define one or more amorphous and/or crystalline phases that may contain iodine. Acetate extractions likely dissolve part (extraction 3) or all (extraction 4) of the calcite in the sediment, which may incorporate iodate. These weak acidic extractions may also partially dissolve other minerals such as amorphous iron oxides. The ammonium oxalate extraction 5 dissolves amorphous iron oxides. The 8 mol/L nitric acid extraction is used to partially dissolve aluminosilicates and phosphates (Sutherland and Tack, 2002), which may contain iodine. Each extraction was shaken for the designated amount of time, centrifuged, and filtered (0.22 μm) before analysis. Extraction reproducibility was measured by duplicate analysis and was ±12%.

Table 2. Artificial pore water used in extractions

Order to Dissolve	Concentration (mol/L)	Reagent	Molecular weight (g/mol)	Mass in 1 liter (g)
1	0.012	$CaSO_4 \cdot 2H_2O$	172.1723	2.0661
2	0.0017	NaCl	58.4430	0.0994
3	0.0004	$NaHCO_3$	84.0068	0.0336
4	0.0034	$NaNO_3$	84.9948	0.2890
5	0.0026	$MgSO_4$	120.3660	0.3130
6	0.0024	$MgCl_2 \cdot 6H_2O$	203.3034	0.4879
7	0.0007	KCl	74.5515	0.0522
Adjust pH to 7.0 to 7.2 with sodium hydroxide or sulfuric acid.				

3.4 Tier 3 Geochemical Characterization

Tier 3 analysis included measurement of the transport and leaching of selected contaminants (total I-129, total I-127, I-129 species, I-127 species) from sediments in column experiments and measurement of iron and manganese surface phases of the sediment that provide a measurement of current or past redox state of the sediment.

3.4.1 Column Leach Experiments

Column leach experiments were conducted to evaluate a) the rate at which iodine is released from field-contaminated sediments at near-field sediment/water ratios, and b) the long-term stability of the remaining

iodine in the sediment after ~130 pore volumes of artificial pore water (APW, Table 2) were leached through the sediments. In contrast to the batch leaching experiments, the column leach experiments had a high sediment/water ratio representative of that in the field, which will likely result in greater iodine species interactions with mineral or organic phases in the sediments, slower dissolution of Fe-oxides, and more iodine reduction reactions which may contribute to release from sediments. One sediment depth with elevated I-129 concentrations was used in column studies (D0006, 206.5 - 207 ft depth), and duplicate column experiments were conducted.

These column studies were conducted after packing moist sediment into 1.58 cm diameter by 15.0 cm length stainless steel columns with 5-μm PTFE end frits. The moisture content of the sediment was determined by weighing 3 to 5 g of moist sediment before and after drying for 48 h at 105°C. The dry bulk density of the sediment was calculated from the dry sediment weight and column volume. The packed column was then water-saturated by injecting artificial pore water (APW, Table 2) into one end of the column until water exited the effluent end of the column. The pore volume, or total water weight in the column, was calculated by the difference of the dry sediment weight and total column volume. The porosity was calculated from the total water weight divided by the column volume. The measured dry bulk density of the two duplicate columns were: 1.476 g/cm^3 and 1.568 g/cm^3 and total porosity 0.417 cm^3/cm^3 and 0.387 cm^3/cm^3, respectively.

The column experiment consisted of injecting APW into the bottom of the column at a constant flow rate to achieve a 1.2-hour residence time (6.1 mL/h) for a total duration of 130 pore volumes. Effluent samples were collected in sufficient number and frequency to measure the change in concentration of the iodine species, which consisted of 12 samples in the first two pore volumes, 12 samples in the next ten pore volumes, 5 samples from 10 to 30 pore volumes, and 5 to 10 samples from 30 to 130 pore volumes. These samples were collected using a timed fraction collector (Isco Foxy 200 or similar) using 4.5-mL tubes (polystyrene). Flow in the column was stopped at 2 pore volumes (72 h stop), 7 pore volumes (70 h stop), 17 pore volumes (146 h stop), and at 125 pore volumes (528 h stop) to evaluate potential change in the iodine release rate from the sediment over time. Initially within the first few pore volumes, aqueous and adsorbed iodine species are released from the sediment, but at later pore volumes, iodine is released from one or more solid phases (i.e., iron oxides and/or calcite or other surface phases) that are slowly dissolving and releasing iodine. The iodine release rate was calculated from the change in aqueous iodine concentration before and after the stop flow event and the length of stop flow time. All effluent samples were measured for total I-129, total I-127, and molybdenum (as molybdate, this species interferes with total I-129 analysis, see Section 3.5). Selected samples in the first four pore volumes that had higher total iodine concentrations were additionally measured for I-129 species (iodide, iodate) and I-127 species.

3.4.2 Selective Iron Extractions

Iron extractions were conducted to quantify the available ferrous (Fe^{II}) and ferric (Fe^{III}) iron surface phases and additionally Mn^{II}/Mn^{IV} phases, both of which are used as an indicator of redox conditions of the sediment. The iron extractions consisted of (a) 1 M $CaCl_2$ (conducted in an anaerobic chamber to decrease iron oxidation), (b) 0.5 M HCl, (c) 0.25 M NH_2OH, 0.25 M HCl, (d) dithionite-citrate-bicarbonate (DCB), and (e) 5 M HCl. The quantity of aqueous Fe^{II} from each extraction was measured using the ferrozine method (Gibbs, 1976) and Fe^{II} plus Fe^{III} after reduction via hydroxylamine hydrochloride solution. Total Fe and Mn in samples was measured by inductively coupled plasma-optical emission spectrometry (ICP-OES). Ferrous iron was divided into four subfractions and determined from the extraction results in the following manner: ion exchangeable Fe^{II} (a), $FeCO_3$ and FeS (b – a), residual Fe^{II} (e – b), and total Fe^{II} (e) (Heron et al., 1994). Similarly, the ferric iron was divided into three subfractions defined by poorly crystalline and amorphous Fe^{III} oxides (c) (Chao and Zhou, 1983), crystalline Fe^{III} oxides (d –c), and total Fe^{III} (e). Manganese extractions were divided into ion exchangeable Mn^{II} (a), $Mn^{II}CO_3$ (b – a), amorphous Mn^{II+IV} (c), and crystalline Mn^{II+IV} (d – c).

3.5 Chemical Analysis Methods

All aqueous analyses were conducted following filtration through 0.45-µm syringe filters. Anions (Br^-, Cl-, F-, NO_3^-, NO_2^-, PO_4^{-3}, SO_4^{-2}) were quantified in aqueous extractions by ion chromatography (IC), with detection limits for each anion listed in Table 3. Metals in liquid extractions were quantified predominantly by inductively coupled plasma-mass spectrometry (ICP-MS), with some metals (Fe, Mn) quantified by inductively coupled plasma - optical emission spectrometry (ICP-OES; Table 3). Ferrous iron was measured by reaction of the aqueous sample with ferrozine (Gibbs 1976) and measurement of the light absorption at 562 nm, following Hach method 8147 (Table 3).

Total uranium in liquid extractions was quantified by ICP-MS and U(VI) aqueous phases were quantified by kinetic phosphorescence analysis (KPA). U(VI) analysis by KPA consists of reacting the 0.45-µm filtered aqueous samples with Uraplex using light from a pulsed nitrogen laser with an excitation wavelength of 425 nm and measurement of the ultraviolet (UV) emission at 515 nm (Brina and Miller 1992). The average lifetime of the U^{VI} as uranyl (UO_2^{2+}) compound emission is 200 to 300 microseconds (µs). A phosphate-based buffer (Uraplex) is used to decrease interferences. The analytical range of uranium measurement for KPA is 0.01 to 30 µg/L.

Select radionuclides, including Tc-99, Sr-90, and Cs-137, were quantified using a liquid scintillation counting (LSC) (Perkin Elmer 3100TR) with liquid extractions. For each isotope, a series of quench standards are used, so the quench curve is used to accurately convert the energy-specific light emission spectra into isotope concentrations. If both Sr-90 and Cs-137 were present in samples, then additional gamma counting will be conducted to quantify Cs-137, and Sr-90 was quantified from the total counts (i.e., both Sr-90 and Cs-137) minus Cs-137 counts within the beta range for the LSC.

The total I-127 and I-129 in aqueous extractions were quantified with a specialized ICP-MS (ThermoScientific iCAP RQ) with collision cell. Samples were diluted in 0.5% Spectrasol (CFA-C, Spectrasol, Inc., Warwich, NY) for total iodine measurement. Total I-127 was present in parts per billion aqueous concentrations that could be quantified directly by ICP-MS with little interference (Figure 3a). TotalI-129 was quantified with detection limits of approximately 5 ng/L using an O_2 collision cell with O_2 addition to decrease interference from Xe-129, which was present in the 99.998% argon carrier gas. Because I-129 concentrations are so low (i.e., parts per trillion levels), there was analytical interference from molybdate (MoO_4^{2-}), which was present in aqueous samples below 1 µg/L but in extraction samples as high as 300 µg/L (e.g., Figure 3a, Kimmig et al., 2021). Molybdate, which was the Mo aqueous species present (Figure 3b), interference increased with the addition of O_2 in the collision cell. The molybdate interference was corrected accurately if Mo was present at < 2 µg/L, so if greater Mo was present, greater sample dilution was needed. This has the result of increasing the minimum detection limits of total I-129. For iodide and iodate species (both I-127 and I-129), an IC was used prior of the ICP-MS analysis to separate ions. Because iodide, iodate, and molybdate were separated, there was less (but still some) interference of molybdate on the I-129 species (Figure 3a).

Total carbon (TC) and inorganic carbon (TIC) in aqueous samples and in the sediment was measured using a carbon analyzer (Shimadzu model TOC-L CSH/CSN E100V). For TC analysis, the liquid sample is combusted by heating it to 680ºC in a furnace to form carbon dioxide (CO_2) gas. For solid samples, the combustion temperature in the SSM-5000A solid sample module is set to 900ºC. The CO_2 gas passes through a non-dispersive infrared (NDIR) gas analyzer where the CO_2 is detected. The analog signal of the NDIR forms a peak and the area is measured by the data processor. For TIC analysis of liquids, the sample is injected into a reaction vessel filled with 25% phosphoric acid at ambient laboratory temperature. This produces CO_2 which is measured by the NDIR detector, as described above. For TIC analysis of solid samples using the SSM-5000A solid sample module, undiluted phosphoric acid is added

to the ceramic sample boat containing the sample at 200°C. TOC is quantified by measurement of TC minus TIC.

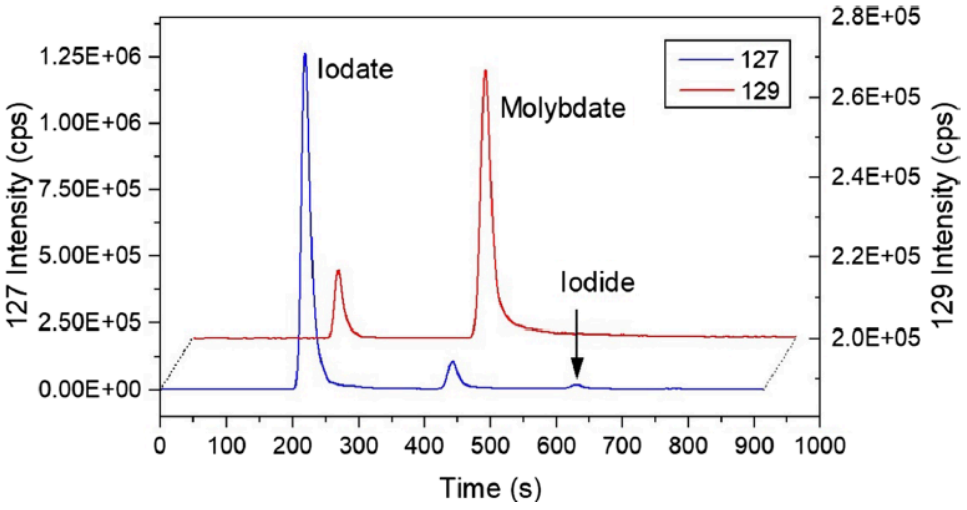

(a)

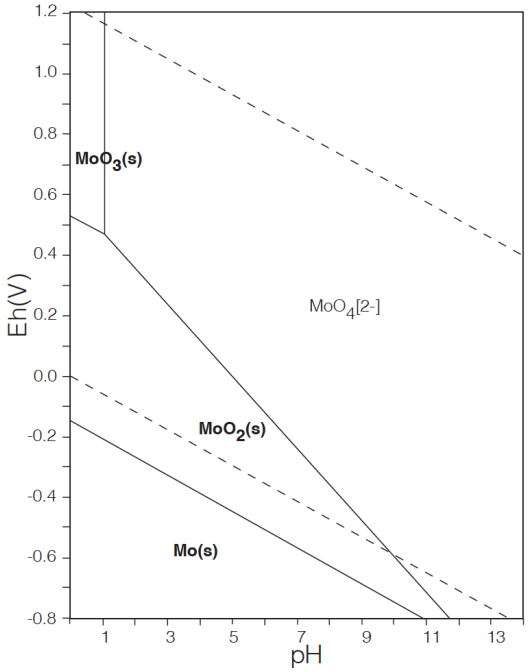

(b)

Figure 3. a) Groundwater sample from well 299-W21-3 with low Mo. Note that interference of Mo was minimal with I-127 species (blue), but significant for I-129 species (red) due to the high Mo concentrations relative to the low I-129 species concentrations, and b) aqueous Mo species Eh-pH diagram showing predominance of molybdate in oxic samples over a wide range of pH.

Table 3. Geochemical analysis methods, hold times, and detection limits.

Data and Instrumentation	Constituents Analyzed	Method	Hold Time[a]	Detection Limit (µg/L)[b]
Aqueous pH by electrode	pH	PNNL-ESL-pH Rev 2	12 hours	± 0.01
Aqueous specific conductance (SpC) by electrode	Specific conductance (SpC)	EPA 9050A	12 hours	10 uS/cm
Anions by ion chromatography	Br^-, Cl-, F-, NO_3^-, NO_2^-, PO_4^{-3}, SO_4^{-2}	PNNL-ESL-IC Rev 1, OP-DVZ-CHPRC-0012	Nitrate, Nitrite: each 48 hrs; PO4: 48 hrs	Br 0.2 mg/L, Cl 0.2, F 0.1, NO_3 0.25, NO_2 0.25, PO_4 0.3, SO_4: 0.3
Total carbon and inorganic carbon in water by carbon analyzer	Total carbon (TC) and total inorganic carbon (TIC)	EPA 9060A, OP-DVZ-CHPRC-0006	28 days	200
U, Tc-99 by ICP-MS	U, Tc-99	PNNL-ESL-ICP-MS Rev 4	6 months	U 0.07, Tc-99 0.3
Total iodine (I-127, I-129) by ICP-MS with collision cell	I-129, I-127	PNNL-ESL-ICP-MS Rev 4	6 months	I-127 1.3, I-129 0.005
U(VI) by Kinetic phosphorescence analysis (KPA)	U(VI)	Brina and Miller 1992, Section 5.12	6 months	0.2
Total carbon and inorganic carbon in sediment by carbon analyzer	TC and TIC	OP-DVZ-CHPRC-0006	none	0.02%
Sr-90, Cs-137 by liquid scintillation counting or beta/gamma counting[c]	Tc-99, Sr-90, Cs-137	OP-DVZ-AFRI-001 RPG-CMC-450, rev 3	6 months	0.5 pCi/g (LSC), 3.6 pCi/mL (Sr-90 beta), 2.0 pCi/mL (Cs-137 gamma)
Metals by ICP-OES or ICP-MS as required for specified detection limits (RCRA and Corrosion indicators)	Ag, Al, As, B, Ca, Cd, Cr, Cu, Fe, Mg, Mn, Mo, Ni, Pb, Se, W, Ti, V	PNNL-ESL-ICP-OES Rev 4, PNNL-ESL-ICP-MS Rev 4	6 months	Ag 0.06, Al 15, As 0.16, B 20, Ca 34, Cd 0.07, Cr 0.06, Cu 0.08, Fe 8.2, Mg 4.1, Mn 2.8, Mo 0.11, Ni 9, Pb 0.05, Se 0.5, W 0.05, Ti 2.6, V 8.5
I-127 Species by IC/ICP-MS	iodate, iodide, other (presumed organic), all as I-127	PNNL-ESL-ICP-MS Rev 4	6 months	2
I-129 Species by IC/ICP-MS with collision cell[d]	iodate, iodide, other (presumed organic), all as I-129	Section 5.16	3 weeks	0.005
Alkalinity by titration	HCO_3^-, CO_3^{2-}	EPA 310.1	12 hours after extraction	5 mg/L
Ferrous iron by spectrophotometer	ferrous iron	Gibbs 1976, Section 5.14	1 day after acidification	1 mg/L

(a) Hold times for characterization of sediments prior to extraction or leaching experiments begin upon opening of sediment cores while hold times for liquid and solid phases from batch and column studies begin at sample collection time.
(b) With no dilution. Highly contaminated sediments may require greater dilution for analysis and increase the detection limits.
(c) If both Sr-90 and Cs-137 are present, gamma counting will be conducted to quantify Cs-137, and Sr-90 will be quantified from the total LSC counts minus Cs-137 counts. Additional column separation and direct beta counting for Sr-90 may also be conducted.
(d) If > 2 µg/L Mo was present, sample dilution is needed which results in an increase in the minimum detection limit.

4.0 Results and Discussion

4.1 Contaminant Concentrations and Sediment Properties (Tier 1)

4.1.1 Anions

Boreholes D0008 and D0006 both showed elevated sulfate and nitrate concentrations in all samples and chloride in most samples (Table 4 and Table 5), indicating that contamination from one or more near-surface leaks has infiltrated deep into the vadose zone. More specifically, chloride concentrations exceeded 100 mg/L in D0008 from 264 to 266 ft depth and in D0006 at 181 to 183 and 206 to 208 ft depths (marked *red* in Table 4), which could accelerate stainless steel casing corrosion (Sedricks 1996). Uncontaminated vadose zone pore water is about 30 mg/L chloride (Szecsody et al., 2017). The pore water specific conductance of 2.8 to 6.0 mS/cm was also higher than uncontaminated pore water (1.6 mS/cm). The current pH of the pore water was slightly alkaline (i.e., 7.6 to 7.9) but within the range of natural Hanford conditions. If the leak source of nitrate, sulfate, and chloride was their acid forms (i.e., HNO_3, H_2SO_4, and HCl, respectively), the moderate to high acid neutralization capacity of the Hanford, Ringold, and Cold Creek sediments would likely have neutralized the acid within tens of feet of the surface (Szecsody et al., 2013).

Table 4. Anion concentrations in water-extracted samples, reported in pore water (mg/L).

Borehole, depth (ft)	HEIS #	Br^- (mg/L)	F^- (mg/L)	Cl^- (mg/L)	SO_4^{3-} (mg/L)	NO_3^- (mg/L)	NO_2^- (mg/L)	PO_4^{3-} (mg/L)	pH	pore H_2O SpC (mS/cm)
D0008A, 264-266	B3TLF5	ND	9.72	169	1265	291	ND	ND	7.87	5.33
D0008A, 264-266dup	B3TLF5	ND	9.66	195	1403	335	ND	ND	--	--
D0008A, 278-280	B3TLF9	ND	2.04	39.1	1261	146	1.46	ND	7.81	2.88
D0008A, 278-280dup	B3TLF9	--	--	--	--	--	--	--	7.77	3.30
D0008A, 284-286	B3TLH3	ND	19.0	53.6	1180	143	ND	ND	7.71	3.43
D0006, 134-136	B3TF28	ND	4.1	65	763	107	ND	ND	7.57	4.13
D0006A, 181-183	B3TF32	ND	6.7	158	1058	362	ND	ND	7.59	5.87
D0006A, 206-208	B3TF36	ND	8.8	137	1080	344	ND	ND	7.70	6.01
D0006A, 206-208dup	B3TF36	ND	6.0	76.7	624	192	ND	ND	7.62	4.37
D0006A, 275-277	B3TF44	ND	0.39	61	871	165	ND	ND	7.80	2.81
MDL[a]	-	0.04	0.04	0.07	0.11	0.07	0.14	0.33	-	-
uncontaminated GW[b]	-	0	0.5	24	67	< 0.5	< 0.3	< 0.4	7.8-8.3	0.20
uncontaminated VZ[c]	-	0	7.6	30	100	< 2	0	0	-	1.6
contaminated VZ[c]	-	0	380	690	30000	1×10^5	22	33	7 - 10	260

(a) MDL – minimum detection level
(b) Lee et al., 2017
(c) Szecsody et al., 2017

Table 5. Anion concentrations in water-extracted samples, reported per gram of sediment.

Borehole, depth (ft)	HEIS #	Br^- (µg/g)	F^- (µg/g)	Cl^- (µg/g)	SO_4^{3-} (µg/g)	NO_3^- (µg/g)	NO_2^- (µg/g)	PO_4^{3-} (µg/g)	pH	pore H_2O SpC (mS/cm)
D0008, 264-266	B3TLF5	ND	0.458	7.97	59.6	13.7	ND	ND	7.87	5.33
D0008, 264-266dup	B3TLF5	ND	0.455	9.18	66.1	15.8	ND	ND	--	--
D0008, 278-280	B3TLF9	ND	0.589	11.3	364	42.1	0.42	ND	7.81	2.88
D0008, 278-280dup	B3TLF9	--	--	--	--	--	--	--	7.77	3.30
D0008, 284-286	B3TLH3	ND	0.476	1.34	29.5	3.57	ND	ND	7.71	3.43
D0006, 134-136	B3TF28	ND	0.1	1.59	18.6	2.62	ND	ND	7.57	4.13
D0006A, 181-183	B3TF32	ND	0.21	4.96	33.3	11.4	ND	ND	7.59	5.87
D0006A, 206-208	B3TF36	ND	0.24	3.74	29.5	9.40	ND	ND	7.70	6.01
D0006A, 206-208dup	B3TF36	ND	0.16	2.04	16.6	5.11	ND	ND	7.62	4.37
D0006A, 275-277	B3TF44	ND	0.15	23.4	332	62.8	ND	ND	7.80	2.81
MDL	-	0.04	0.04	0.07	0.11	0.07	0.14	0.33	-	-

A comparison of the anion concentrations reported here to results reported over a greater range of depths for D0006 (from GEL labs data, reported in the Hanford Environmental Information System, HEIS), shows similar trends with chloride and nitrate peaking at 200 to 230 ft depth, and the sulfate at shallower depth, peaking at 130 to 200 ft depth. The chloride, nitrate, and sulfate concentrations differ between Pacific Northwest National Laboratory (PNNL) and GEL samples as sample depths are different. Cr also showed elevated levels greater than 200 ft depth (Figure 4). Although only major anion and Cr data comparison is presented here, there are additional radionuclide depth profiles are reported in the following section.

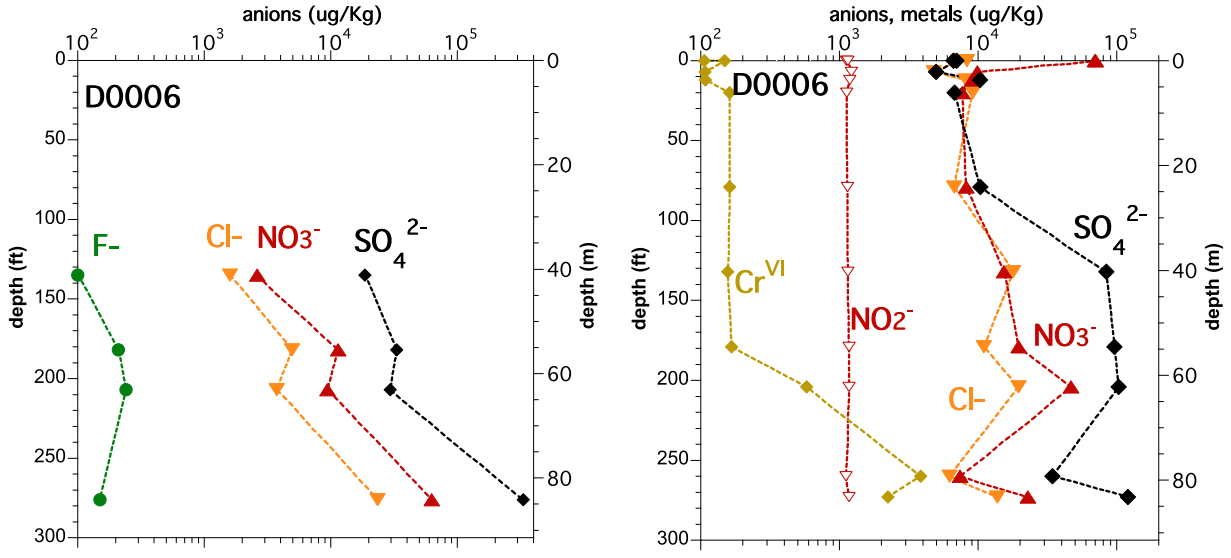

Figure 4. Anion concentrations with depth for D0006 reported by PNNL (a) and GEL labs (b).

The nitrate profile in D0008 (Fig. 5a) showed elevated concentrations at the 260 to 280 ft depth, which may have been a result of a surface spill or elevated groundwater and correlated with finer sediments of higher water content (Section 4.1.3). Because of the proximity of boreholes D0008 and D0006 to the

242A evaporator, a comparison of D0006 depth profile is made to a depth profile from beneath 242A liquid discharge (borehole C4106, Figure 5b). The D0006 profile is not the same as C4106 profile from drilling conducted in 2003 under the 216-A-37-1 crib, which received liquid effluent waste from the 242A evaporator. That profile depicted in Figure 5 includes both total nitrogen and nitrate is the result of NH_4OH discharge, where strong sorption of NH_4^+ to sediment and slow oxidation to nitrate was observed. A portion of the N species to discharge to groundwater along with tritium in the 1980s, leaving a portion of N in the first 100 ft of the vadose zone (Szecsody et al., 2020a).

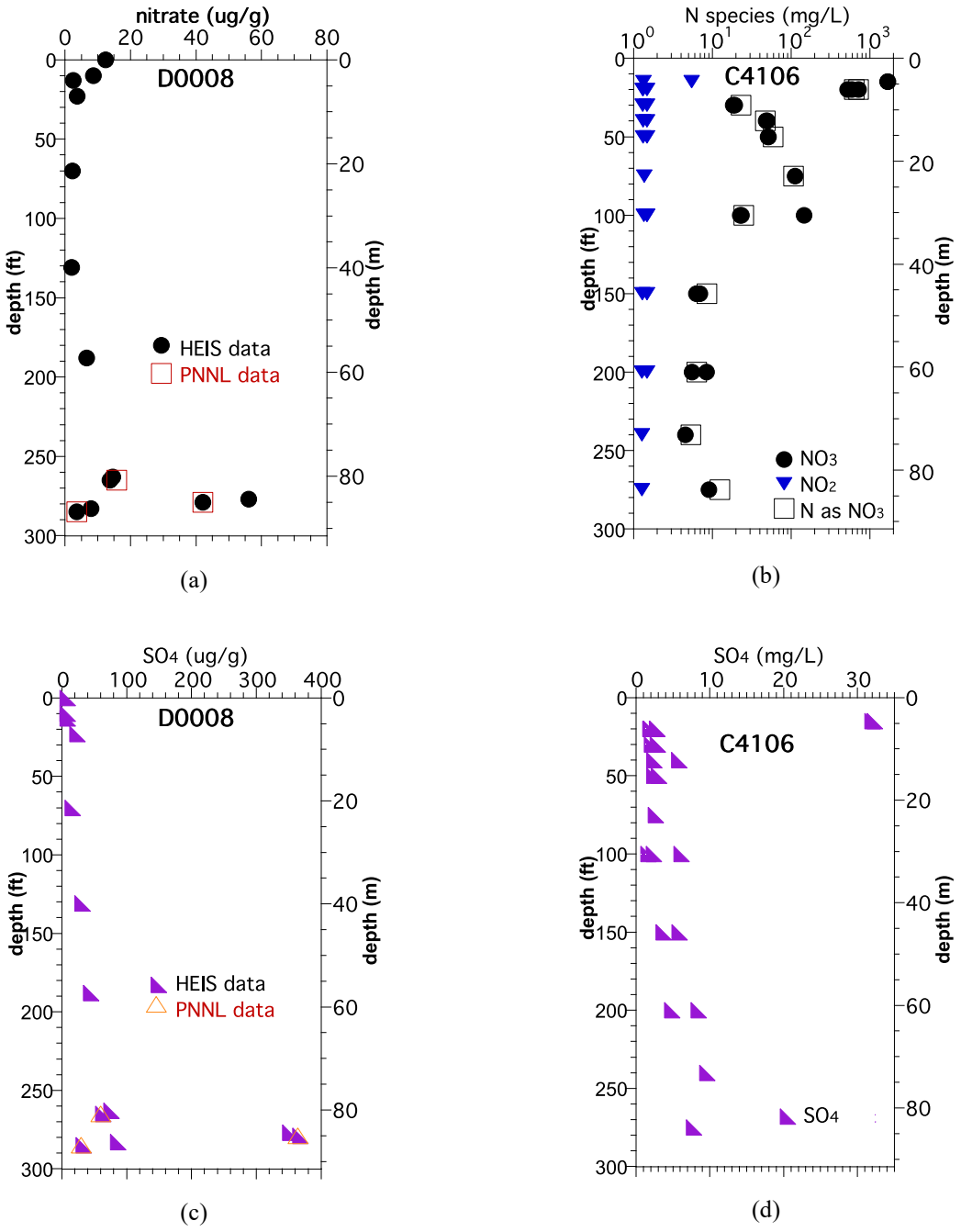

Figure 5. Nitrate and sulfate depth profile for D0008 (a and c) and nearby depth profile from C4106, under the nearby the 216-A-37-1 crib.

The sulfate profile in D0008 was also elevated at 280 ft depth, possibly from contaminated groundwater, as there is only a slight increase in sulfate with depth shallower in the vadose zone. In contrast, C4106 received predominantly NH_4OH waste discharges (and some sulfate) and shows slightly elevated sulfate concentrations throughout the vadose zone. This wastewater depth profile was known to reach groundwater, so this profile likely indicates some sulfate precipitation, exchange with mineral surfaces or presence in residual pore water.

4.1.2 Radionuclides

Most radionuclide concentrations measured in water and acid extractions from D0006 and D0008 were at or near natural levels (for uranium and Th-232) or detection limits (for Tc-99, Sr-90, and Cs-137) (Table 6). The only radionuclide with elevated concentrations was I-129 which was measured in D0006A at the 206 to 208 ft depth. The I-129 in D0006A at 275 to 277 ft depth was slightly above detection limits. Based on these results, Tier 2 (and subsequently Tier 3) analysis was conducted only on the D0006A 206 to 208 ft depth sample. In terms of the depth profile, radionuclide data for D0006 for both PNNL and GEL data, shows shallow tritium, but deep Tc-99 (and nitrate and sulfate, Figure 4). Comparing the observed radionuclide and anion depth profile (Figure 6b) to a hypothesized single surface source based on their relative retardation factors (Figure 6c) shows differences. The observed vertical profile suggests more than one release, where there is a later leak of tritium and possibly nitrate (accounting for the shallow nitrate and tritium) at the surface because tritium should move unretarded (similar to nitrate, slightly faster than chromate, Truex et al., 2017, Szecsody et al., 2019) and faster than other radionuclides (Routson et al., 1981, Szecsody et al., 2018) as shown in (c).

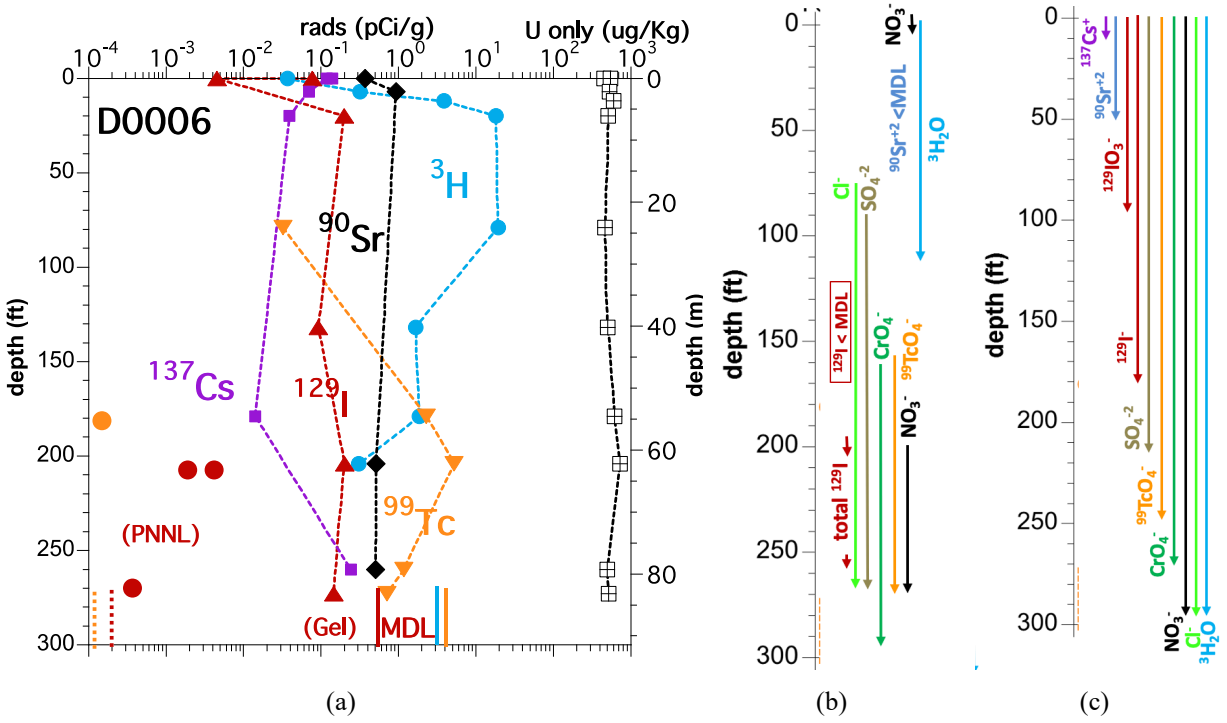

Figure 6. Radionuclide depth profile for borehole D0006 with *circles* representing PNNL results and *triangles* representing GEL results and dashed and solid lines representing MDLs for PNNL and GEL results, respectively (a), approximate depth profiles for radionuclides, metals, and anions (b), and approximate expected depth profile assuming a single surface discharge (c).

Table 6. Radionuclide concentrations measured in boreholes D0008 and D0006.

		Water Extracts								Acid Extracts					
Borehole, depth (ft)	HEIS #	U-238 (µg/g)	U(VI) (µg/g)	Tc-99 (µg/g)	Sr-90 (pCi/g)	Cs-137 (pCi/g)	I-129 (µg/g)	I-129 (pCi/L)	I-127 (µg/g)	U-238 (µg/g)	U(VI) (µg/g)	Tc-99 (µg/g)	Sr-90 (µg/g)	Cs-137 (µg/g)	Th-232 (µg/g)
D0008A, 264-266	B3TLF5	$9.26x10^{-5}$	ND	ND	ND	ND	ND	ND	$8.46x10^{-4}$	0.224	0.179	ND	ND	ND	1.41
D0008A, 278-280	B3TLF9	ND	ND	ND	ND	ND	ND	ND	$6.78x10^{-4}$	0.503	0.467	ND	ND	ND	2.44
D0008A, 278-280 dup	B3TLF9	$1.85x10^{-4}$	ND	ND	ND	ND	ND	ND	$7.31x10^{-4}$	0.505	0.474	ND	ND	ND	2.41
D0008A, 284-286	B3TLH3	ND	ND	ND	ND	ND	ND	ND	$1.47x10^{-4}$	0.209	0.165	ND	ND	ND	1.19
D0006, 134-136	B3TF28	ND	ND	ND	ND	ND	ND	ND	$5.03x10^{-4}$	0.244	0.235	ND	ND	ND	1.56
D0006A, 181-183	B3TF32	ND	ND	$3.41x10^{-5}$	ND	ND	ND	ND	$6.41x10^{-4}$	0.237	0.222	ND	ND	ND	1.63
D0006A, 206-208	B3TF36	ND	$6.7x10^{-5}$	ND	ND	ND	$4.98x10^{-5}$	335	$7.34x10^{-4}$	0.253	0.249	ND	ND	ND	1.75
D0006A, 206-208 dup	B3TF36	ND	$6.2x10^{-5}$	ND	ND	ND	$2.62x10^{-5}$	176	$4.35x10^{-4}$	0.294	0.278	ND	ND	ND	1.82
D0006A, 275-277	B3TF44	ND	ND	ND	ND	ND	$2.28x10^{-6}$	1.32	$9.15x10^{-4}$	0.811	0.94	ND	ND	ND	2.86
MDL		$7x10^{-5}$	$5x10^{-4}$	$7x10^{-5}$	1.7±0.4		$1x10^{-6}$	-	$1.0x10^{-4}$	$2.0x10^{-3}$	$6x10^{-4}$	$7x10^{-5}$	$2x10^{-4}$	$1x10^{-4}$	
uncontaminated GW[(a)]		$1x10^{-4}$	$1x10^{-4}$	0	0	0	0	-	$0.6 – 2x10^{-3}$	0.2	< 0.2	0	0	0	
uncontaminated VZ[(b)]		$7x10^{-4}$	$7x10^{-4}$	0	0	0	0	-	0.01	0.3-0.5	-	0	0	0	
contaminated VZ[(b)]		0.22	0.22	$6x10^{-3}$	$1x10^{-5}$	0	0.01	-	0.1	0.5 - 7000	-	$2x10^{-5}$	0.001		

(a) Lee et al., 2017
(b) Szecsody et al. 2017
ND = non-detect

4.1.3 Sediment Physical Properties

The grain size distribution of the seven sediments analyzed showed five were silty or gravely sand and two were finer grained silt samples (Table 7). Finer grained samples were from the 275 to 278 ft depths in both D0006 and D0008 were at or near water-saturated conditions. With a higher water content in the silt samples, mobile contaminant concentrations tend to be greater when reported per gram of sediment, which was observed for the D0006 275 ft and D0008 278 ft depths (Table 5). Grain size distributions for the coarser sediments showed a bimodal distribution (i.e., two predominant grain sizes), which may be indicative of more than one depositional environment, such as a low and medium energy stream deposit (Figure 7 and Figure 8).

Table 7. Physical properties of sediment samples.

Borehole, depth (ft)	HEIS #	Dry Bulk Density (g/cm^3)	Moisture (%)	Clay (%)	Silt (%)	Sand (%)	Gravel (%)	Description	Unit
D0006, 134-136	B3TF28	2.23	2.25	1.56	13.6	89.5	2.5	sand, trace of silt	H1
D0006A, 181-183	B3TF32	2.26	2.82	1.57	7.63	85.4	5.4	sand, trace silt, gravel	H2
D0006A, 206-208	B3TF36	loose	2.63	1.22	13.6	84.1	1.1	sand, trace of silt	H2
D0006A, 275-277	B3TF44	1.71	27.6	19.1	80.1	0.9	0.0	silt with some clay	CCu (silt)
D0008, 264-266	B3TLF5	1.80	4.50	1.05	18.2	80.8	0	silty sand	H2
D0008, 278-280	B3TLF9	1.60	22.4	10.2	78.3	11.5	0	silt with some clay and sand	CCu (silt)
D0008, 284-286	B3TLH3	1.56	2.44	0.869	9.27	51.8	38.1	gravely sand with trace of silt	CCu (gravel)

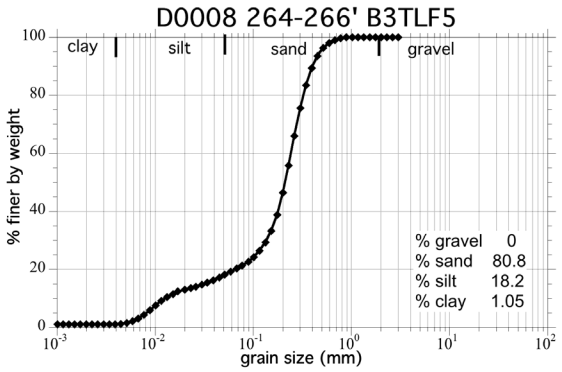

(a)

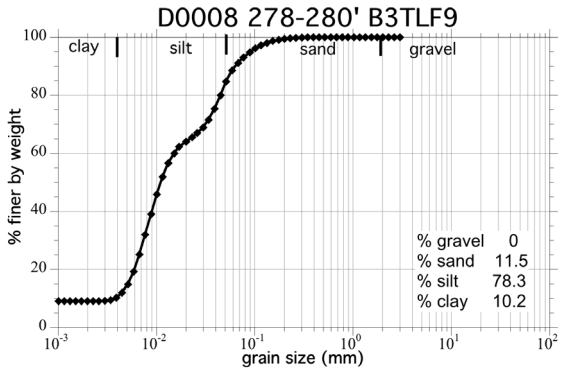

(b)

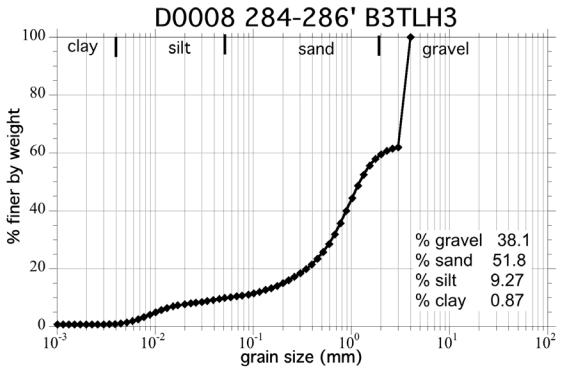

(c)

Figure 7. Grain size distributions for D0008.

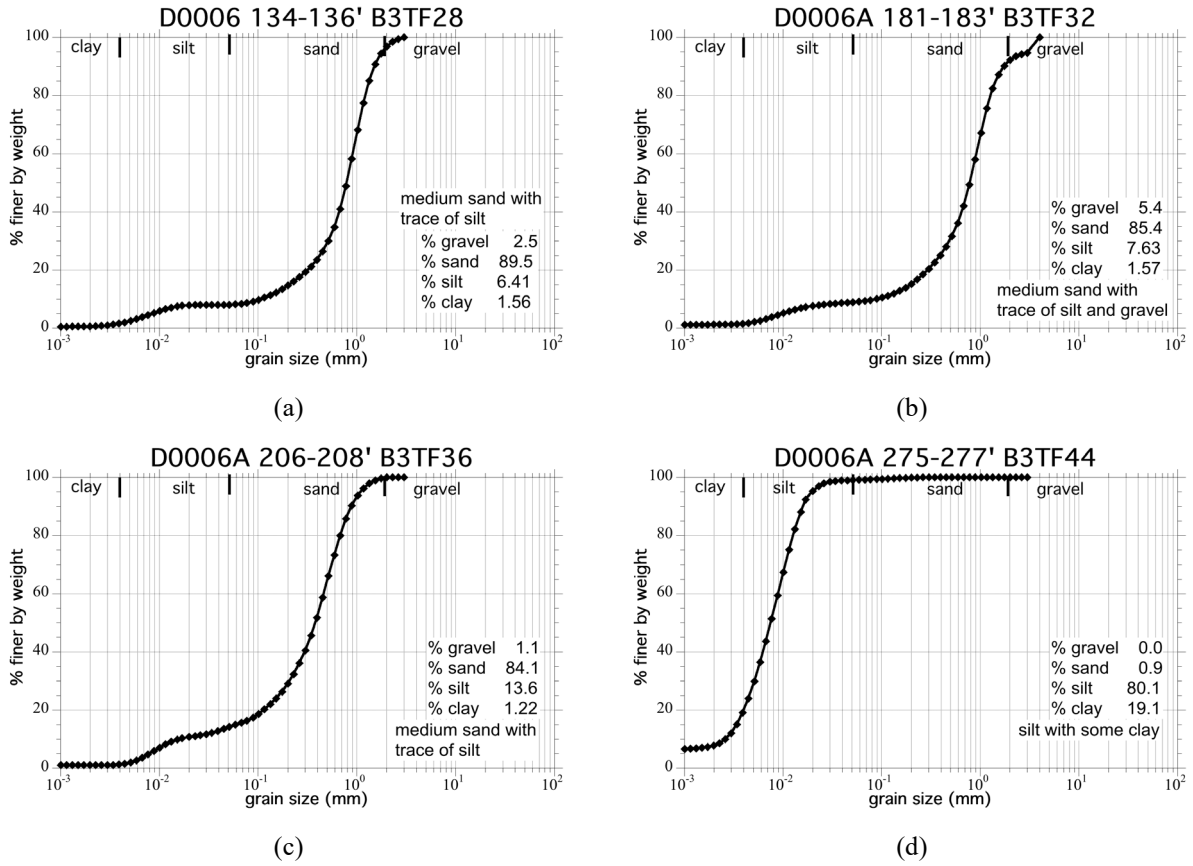

Figure 8. Grain size distributions for D0006.

4.2 Contaminant Species and Geochemical Setting (Tier 2)

4.2.1 Geochemical Constituents

An understanding of the full geochemical setting for contaminants is needed to quantify aqueous and solid phase species and ultimately predict contaminant migration. For example, both aqueous and solid phase carbonate concentrations highly influence the transport of uranium, and to some extent iodine. In Hanford groundwater (which is Ca, Mg-carbonate saturated), aqueous uranium is complexed with carbonates (i.e., several Ca-uranyl-carbonate species present at pH ~8), which exhibit low sorption. In low aqueous carbonate conditions, which are present in the Hanford 300 Area and under the U-8 crib (both acidic disposal sites), aqueous uranium solubility is lower, and uranium will precipitate at elevated concentrations. In the natural Hanford subsurface, with an average of 1.9% and 0.7% calcite in the Hanford and Ringold formations respectively (Xie et al., 2003), significant uranium and iodine will co-precipitate with calcite. In contrast, at acidic disposal sites with low calcite, solid phase uranium is not present in association with calcite due to the increased solubility of both U and carbonates.

For this study, Tier 2 analysis is focused on I-129 and I-127 species, which are primarily iodide and iodate in the absence of significant TOC (Zhang et al. 2013). Although there are no aqueous iodine-carbonate complexes, there are some solid phase interactions. Iodate can incorporate into calcite, while iodide cannot (Lawter et al. 2018). Therefore, measurement of aqueous and solid phase TIC and TOC is useful to predict the migration of I-129 and I-127 species. Natural pore water would be dominated by carbonate, with lesser amounts of sulfate and chloride, and trace (< 1 mg/L) nitrate from plant respiration.

Analysis of the solid phase TIC in the sediment (0.192% carbon) calculates to ~1.65% calcite (Table 8) or 1.1% by X-ray diffraction analysis of the sediment. The TOC content was below detection limits (0.005%), which was expected for a sediment sample from this depth in terms of natural TOC. This lack of TOC also indicates no measurable organic waste solvent contamination.

Cation and anion analysis of the pore water for D0006A 206 to 207 ft depth indicate significant contamination compared to natural pore or groundwater (Table 8 and Table 9). Full anion analysis of the D0006A 206 to 207 ft depth (first two lines, Table 8) was similar to that previously reported for partial anion analysis (second two lines, Table 8, from Table 4), but additionally with aqueous carbonate measured by carbon analyzer as well as alkalinity by titration. This depth was dominated by sulfate at > 10 times natural concentrations and also elevated nitrate. As both are likely from sulfuric and nitric acid, common associated cations are Na and K from acid neutralization using NaOH and KOH. Pore water cation analysis (Table 8) show greatly elevated Na and K concentrations and some elevated Ca and Mg. Ca^{2+} and Mg^{2+} sorb strongly to Hanford sediments (Kd ~25 cm^3/g, Rf ~120) and are not common waste constituents. However, acidic solutions disposed near the surface would be neutralized in shallow sediments (tens of feet depth) by calcite and clay dissolution (and ion exchange), which would result in elevated carbonate and Ca and Mg at depth (and depleted calcite and aforementioned ions in shallow sediments). Elevated Si (160 mg/L in pore water) is also indicative of dissolution of clays or other silicates.

Major cations/metals were also measured in acid extractable sediments to evaluate whether there were direct indications of products of stainless-steel corrosion or other impacts from waste constituents (Table 10 and Table 11). Two types of stainless steel that were likely used in casing are 316L and 304 (also called 18/8). The 316L stainless steel is composed of 16-18% Cr, 10-14% Ni, 2-3% Mo, 1% Si, and 2% Mn, whereas 304L stainless steel is composed of 18% Cr, 8% Ni, Mn 2%, and 0.75% Si, both with (< 0.1% of P, S, and C). Acid dissolution of the steel most likely at welds would not leach metals in proportion to the composition, as the aqueous speciation and precipitates differ for each metal. However, elevated Fe, Cr, Ni, Mo, Mn, and Si above what is naturally found in sediment minerals (i.e., total, by acid dissolution) may be a direct indication of well casing corrosion or transport from a shallow spill (i.e., metal disposal in the 200-E-286 ditch and acidic infiltration from a tank spill would also leach steel components to depth). Acid extractions and metals analysis of the D0006A 206.5-207 ft depth sediment did show elevated Cr, although Fe, Mn, Mo, and Ni were all within natural sediment range for Hanford (DOE, 1993). Previous characterization of natural Cr in Hanford and Ringold formations show an average 18.5 μg/g (range 2.9 to 33.2 μg/g, DOE 1993), with only a small fraction (< 5%) being mobile as aqueous or adsorbed chromate, where the mobile chromate is more likely from contamination (Szecsody et al. 2019, 2017, Truex et al. 2017). However, pore water chromate was present at 0 to 180 ft depth at a low (but above natural concentration), then increased significantly at 180 to 280 ft depth (Figure 4b), which is more consistent with a surface spill and transport of chromate to depth.

Table 8. Water extracted anions and solid phase carbon.

Borehole, depth (ft)	HEIS #	Br- (mg/L)	F- (mg/L)	Cl- (mg/L)	SO_4^{2-} (mg/L)	NO_3^- (mg/L)	NO_2^- (mg/L)	PO_4^{3-} (mg/L)	CO_3^{2-} (mg/L)	Alkalinity (mg/L)	pH	TIC (% g/g)	TOC (% g/g)	Calcite (%)[c]
D0006A, 206.5-207	B3TF37	ND	ND	164	1215	650	ND	ND	108	< MDL	7.66	0.192	< MDL	1.60/1.1
D0006A, 206.5-207 dup	B3TF37	ND	ND	172	1318	588	ND	ND	146	< MDL	7.64	0.209	< MDL	1.74
D0006A, 207-207.5	B3TF36	ND	9.03	141	1109	353	ND	ND			7.70			
D0006A, 207-207.5 dup	B3TF36	ND	6.02	76.7	624	192	ND	ND			7.62			
MDL			0.04	0.07	0.11	0.07	0.14	0.33	2.5			0.005	0.005	0.04
uncontaminated VZ[a]		0	7.6	46	230	95	0	0	166					
uncontaminated GW[b]		0	0.5	24	67	< 0.5	< 0.3	< 0.4	166					

(a) Szecsody et al., 2017
(b) Lee et al., 2017
(c) first value is calculated from the total inorganic carbon (TIC), second value (1.1%) is solid phase X-ray diffraction analysis (for information only)

Table 9. Water extracted cations.

Borehole, depth (ft)	HEIS #	Extract Type	Ca (mg/L)	Mg (mg/L)	K (mg/L)	Na (mg/L)	Si (mg/L)	Sr (mg/L)	S (mg/L)
D0006A, 206.5-207	B3TF37	water	482	177	265	482	160	2.1	405
D0006A, 206.5-207 dup	B3TF37	water	464	187	261	453	169	2.1	456
uncontaminated GW[a]			53	13.4	8.2	26	15	0.1	22.2
uncontaminated VZ[b]			36	10	47	50	9	<0.05	70

(a) Lee et al., 2017
(b) Szecsody et al., 2017

Table 10. Acid extractable major metals, reported per gram of sediment.

Borehole, depth (ft)	HEIS #	Extract Type	Ca (mg/g)	Mg (mg/g)	K (mg/g)	Na (mg/g)	Si (mg/g)	Sr (mg/g)	S (mg/g)	Fe (mg/g)	P (mg/g)	Mn (mg/g)	Ti (mg/g)	**Al (mg/g)**	**Ba (mg/g)**
D0006A, 206.5-207	B3TF37	acid	10.2	6.32	2.29	0.409	0.022	0.044	0.043	16.8	0.390	0.233	0.636	8.70	0.108
D0006A, 206.5-207 dup	B3TF37	acid	10.8	5.80	2.16	0.280	0.021	0.042	0.049	15.4	0.419	0.298	0.662	8.08	0.089
MDL		acid	0.2	0.2	0.5	0.05	0.005	0.003	0.002	0.007	0.05	0.0006	0.005	0.02	0.004
uncontaminated VZ[a]			6-11	3-7	0.8-2.2	0.2-0.5	0.1-0.5	0.018	.03-.1	8-34	0.8-2.2	0.2-0.55	0.6-3	6-16	.06-.1

(a) DOE, 1993

Table 11. Acid extractable trace metals, reported per gram of sediment.

Borehole, depth (ft)	HEIS #	Extract Type	Bi (mg/g)	Cd (mg/g)	Cr (mg/g)	Co (mg/g)	Cu (mg/g)	Ga (mg/g)	Pb (mg/g)	Li (mg/g)	Ni (mg/g)	Re (mg/g)	Sn (mg/g)	V (mg/g)	Zn (mg/g)	Zr (mg/g)
D0006A, 206.5-207	B3TF37	acid	0.00141	9.27×10^{-4}	0.0128	0.0050	0.0063	0.00271	0.00163	0.0168	0.0124	5.7×10^{-4}	0.0190	0.0190	0.0246	0.00533
D0006A, 206.5-207 dup	B3TF37	acid	0.00171	0.00190	0.0174	0.00563	0.00904	0.00351	0.00159	0.0166	0.0127	6.6×10^{-4}	0.0229	0.0260	0.0275	0.00648
MDL				0.0005	0.001	0.001	0.002	0.0004	0.001	0.005	0.007	1.2×10^{-4}	0.002	0.002	0.005	0.004
uncontaminated VZ[(a)]			--	<MDL	.003-.01	.006-.02	0.01-.03	--	.001-.009	<MDL	0.07-.15	--	--	.05-.1	.03-.06	.01-.04

Below MDL: At, As, Be, B, Mo, Se, Ag, Th
uncontaminated Mo 0 - 0.002 mg/g
(a) DOE, 1993

4.2.2 I-129 and I-127

Elevated total I-129 levels in Tier 1 analysis of D0006A, 206 to 208 ft depth sediments triggered more detailed Tier 2 characterization of this sample to evaluate iodine mobility. Sequential extractions for total I-129 and associated I-127 are used to evaluate the fraction of total iodine that is mobile (i.e., in aqueous or adsorbed phases), in high solubility precipitates (potentially mobile) or low solubility precipitates (not mobile). In addition, iodine speciation of extracted samples for both I-129 and I-127 (i.e., iodide and iodate) was also conducted, as iodide exhibits less sorption (i.e., K_d < 0.1 cm^3/g) than iodate (i.e., K_d ~ 0.4 cm^3/g), meaning that it is somewhat more mobile (Szecsody et al., 2018, 2020b).

The acidic sequential extractions for total I-127 showed ~23% was mobile (i.e., aqueous and adsorbed), and the largest fraction of total I-127 was associated with solid phases that were extracted with pH 5 acetate (extraction 3, 21%) or pH 2.3 acetic acid (extraction 4, 46%) (Table 12 and Figure 9). This may indicate iodine incorporated into calcite, as recent laboratory studies have demonstrated (Lawter et al., 2018). The 1000-h carbonate extraction has been previously used to exchange solid phase contaminants that are associated with calcite, such as uranium (Zachara et al., 2007, Kohler et al., 2004). The 1000-h extraction removed approximately 49% of the total acid extractable I-127. 1-D column leach experiments (Section 4.3.1) showed only a small fraction (< 4%) of total I-127 leached in 130 pore volumes.

Compared to the acidic sequential extractions, the TMAH extraction removed 80% more I-127 from the sediment, so additional surface phases are present that release I-127 under alkaline conditions. These results are similar to previously reported I-127 extractions in Hanford sediments (Szecsody et al., 2020b).

I-127 speciation on all extracted liquids shows iodine is predominantly present as iodide (> 95%), with only low concentrations of iodate present (Table 12). The predominance of iodide-127 in vadose zone pore water is previously reported (Szecsody et al., 2018, 2020b), and in contrast to the predominance of I-127 as iodate in groundwater (Zhang et al., 2013).

Table 12. I-127 total and iodine species analysis of sequential and parallel liquid extractions.

Borehole, depth (ft)	HEIS #	H_2O ex. (µg/g)	ex. 1 (µg/g)	ex. 2 (µg/g)	ex. 3 (µg/g)	ex. 4 (µg/g)	ex. 5 (µg/g)	ex. 6 (µg/g)	Total (µg/g)	1000h (µg/g)	TMAH[a] (µg/g)
D0006A, 206.5-207	B3TF37	0.0194	0.0332	0.0029	0.03284	0.070	0.0031	0.0118	0.1539	0.0752	0.276
D0006A, 206.5-207 dup	B3TF37	0.00205	0.0011	0.0010	0.00312	0.008	0.0031	0.0118	0.0283	0.1079	0.260
D0006A 207, post leach	B3TF37		0.0217	0.0005	0.0026	0.0055	0.0180	0.0265	0.0747[d]		
D0006A, 207-207.5	iodate[b]	< MDL	7.3×10^{-4}	1.5×10^{-4}	< MDL	< MDL	--	--		< MDL	<MDL
D0006A, 207-207.5 dup	iodate[b]	< MDL	5.8×10^{-4}	4.6×10^{-4}	2.0×10^{-4}	< MDL	--	--		< MDL	< MDL
D0006A, 207-207.5	iodide[b]	0.022	0.0340	0.033	0.030	0.077	--	--		0.083	0.292
D0006A, 207-207.5 dup	iodide[b]	0.00081	0.0029	0.004	0.005	0.009	--	--		0.114	0.232
MDL		7.4×10^{-5}	7.4×10^{-5}	7.4×10^{-5}	7.4×10^{-5}	7.4×10^{-5}	7.4×10^{-5}	$7.x10^{05}$	7.4×10^{-5}	7.4×10^{-5}	5.0×10^{-5}
contaminated GW[c]	W22-114	0.17									
uncontaminated GW	699-36-70A	0.11									
contaminated VZ	C9507 104'	0.057	0.06	0.08	0.32	0.47	0.15	1.2	2.1		2.5

(a) TMAH I-127 spike recovery was outside ±20%
(b) Iodate + iodide was not within ±20% of total I-127. Species are not corrected for Mo interference.
(c) Szecsody et al., 2017
(d) Total post leach. T1 leached 0.00289 µg/g, T2 leached 0.00525 µg/g total I-127.

The total I-129 values in various extractions were difficult to analyze at the reported low concentrations due to interference with co-extracted molybdenum. Aqueous I-129 was 0.00031 to 0.00074 µg/g, which is low compared to previous aqueous extracted I-129 in contaminated Hanford sediments (0.001 to 0.01

µg/g; Szecsody et al., 2018, 2020b). The total TMAH extracted I-129 for this sediment (0.0015 µg/g) was also low relative to other contaminated Hanford sediments (0.04 to 0.1 µg/g).

The aqueous total I-129 was 25% to 50% of the TMAH-extracted total I-129, in contrast to I-127, where the aqueous I-127 was 5% to 12% of the TMAH-extracted I-127. The I-129 was below detection limits in sequential acidic extractions 2 through 6, and the 1000-h carbonate extraction mainly due to the presence of high molybdate, which required samples to be diluted so Mo was < 2 µg/L, and subsequently increased the minimum detection limit for I-129. Measured Mo concentrations in extractions did indicate higher concentrations in the acidic sequential extractions (Table 13). Lower detection limits for total I-129 in the presence of Mo are possible with the future development of a separation column to strip out the molybdate before I-129 analysis.

Based on these results, I-129 may not be present in the same surface phases as I-127 (Figure 10). If I-129 and I-127 were present in the same aqueous, adsorbed, and solid surface phases, then analysis of I-127 transport would provide useful information on the potential migration of I-129. However, because each of these isotopes represent different sources of iodine, it is reasonable that they may exist in different solid phases.

A comparison of the I-127/I-129 isotopic ratios in the A-AX tanks to subsurface samples provides some information about pore water dilution or contribution of multiple sources. The I-127/I-129 isotopic ratios in the Hanford tanks are 2.3 to 7.3 (241-BY-107 and 241-C-104), and 0.79 to 1.27 for a second group (AN-104, AP-101, AW-101, BY-108, S-102, S112; Reynolds, 2021). For the A tanks (AN-104, AP-101, AW-101), the I-127/I-129 isotopic ratio is 0.32 ± 0.13. Given the subsurface I-127/I-129 isotope ratio in D0006A at 206.5 to 207 ft depth of 63 for the deionized water extraction and 40 to 45 for the artificial pore water extraction (Table 13), the change from a ratio of 0.32 is likely due to the addition of mainly natural I-127 from sediments. The change in I-127/I-129 isotopic ratio (assuming the AN/AP/AW tank ratio is applicable to AX) indicates a dilution of 126 to 200. Dilution of the iodine in the tanks with other waste streams (i.e., 200-E-286 trench) would dilute concentrations but not change the I-127/I-129 isotopic ratio (assuming trench waste contained no iodine). In contrast, for total iodine extractions of the sediment and pore water, the I-127/I-129 isotopic ratio was 210 (total for acid extractions) and 190 (TMAH extraction), indicating considerable additional natural I-127 dissolved from sediment minerals. It is hypothesized that I-127 dilution of pore water from a surface release will increase with depth, so the I-127/I-129 isotopic ratio should increase from tank values (0.32) to higher values (i.e., 45 at 207 ft depth, for example). Differences in the change in the I-127/I-129 ratio with depth between boreholes might indicate different I-129 or I-127 sources. Given the 126 to 200 times dilution, this indicates the pore water chloride concentration of 77 mg/L could have been 9700 to 15000 mg/L in the 200-E-286 trench.

Table 13. I-129 total analysis of sequential and parallel liquid extractions.

Borehole, depth (ft)	HEIS #	H2O ex. (µg/g)	ex. 1 (µg/g)	ex. 2 (µg/g)	ex. 3 (µg/g)	ex. 4 (µg/g)	ex. 5 (µg/g)	ex. 6 (µg/g)	Total (µg/g)	1000h (µg/g)	TMAH (µg/g)
D0006A, 206.5-207	B3TF37	3.1×10^{-4}	7.4×10^{-4}	< MDL	< MDL	< MDL	< MDL	< MDL	7.4×10^{-4}	< MDL	1.4×10^{-3}
D0006A, 206.5-207 dup	B3TF37	< MDL	2.9×10^{-5}	< MDL	< MDL	< MDL	< MDL	< MDL	2.9×10^{-5}	< MDL	4.91×10^{-3}
D0006A, 206.5-207 I-127/I-129 ratio		63	40-45	--	--	--	--	--	210	--	190
D0006A 207, post leach	B3TF37		< MDL	< MDL	< MDL	< MDL	< MDL	< MDL			
D0006A, 207-207.5	B3TF36	$5E \times 10^{-5}$									
MDL		3.2×10^{-5}	3.2×10^{-5}	1.6×10^{-4}	1.6×10^{-4}	1.6×10^{-4}	1.6×10^{-4}	1.6×10^{-3}	3.2×10^{-5}	3.2×10^{-5}	3.2×10^{-4}
Mo (ug/L)	B3TF37	4.1	4.6	4.6	15.4	ND	ND	46.1			
contaminated GW[(a)]	W22-114	0.04									
contaminated VZ[(b)]	C9507 104'	0.0015							0.031		0.01

(a) Lee et al., 2017
(b) Szecsody et al., 2018

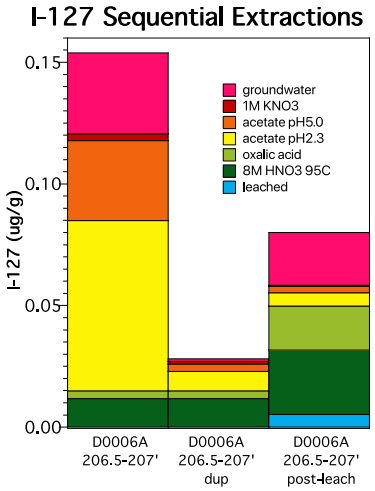

Figure 9. Pre- and post-leach total I-127 sequential extractions.

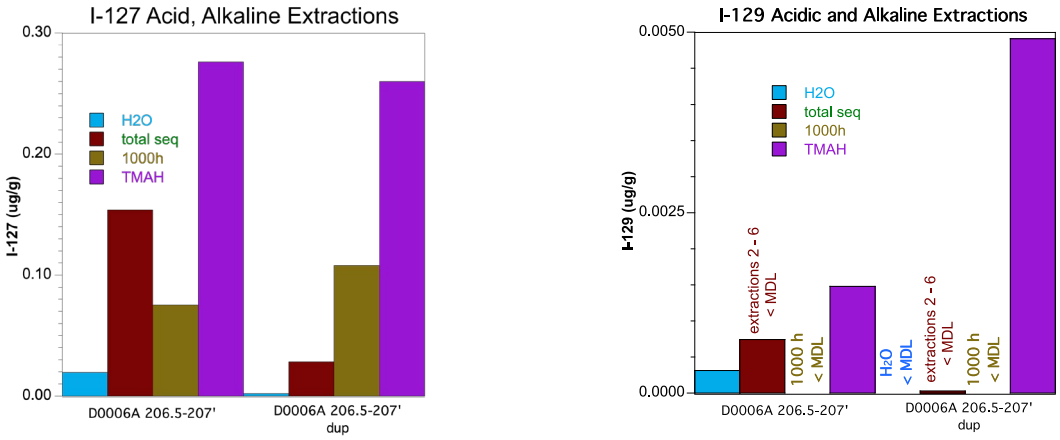

Figure 10. Comparison of the total I-127 (a) and I-129 (b) for different extractions.

4.3 Contaminant (I-129) Transport (Tier 3)

4.3.1 Leach Experiments with I-129, I-127, and Mo Analysis

1-D column leach experiments were conducted in Tier 3 to measure both the mass and rate of I-129 released from the D0006A 206.5-207 ft depth sediment. To meet those objectives, artificial pore water (APW) was injected at a constant flow rate for 130 pore volumes, and effluent samples were collected to measure total I-129, I-129 species, total I-127, I-127 species, and molybdate. Because iodide (as I-127) is naturally present in the sediment (Table 12), a larger number of effluent samples were collected in the first few pore volumes to capture iodide and iodate behavior for both I-127 and I-129. Two separate 1-D column leach experiments were conducted with the D0006A sediment.

Results of both leach experiments showed only a few samples above the detection limits for total I-129 (Figure 11a and b). Measured concentrations of 0.08 to 0.42 µg/L were similar to values previously measured in aqueous extractions (i.e., 0.31 and 0.33 µg/L, Table 13). The minimum detectable limits

(MDLs) for each sample showed change resulting from different dilutions needed for different samples, depending on the molybdenum concentration. There were four stop flow events in both experiments, which resulted in an increase in molybdenum (described below), which unfortunately increased the total I-129 detection limits. Therefore, leach experiments were not useful for evaluating leached I-129 mass nor the I-129 leach rate from sediment.

In contrast, total I-127 was quantified in all effluent samples along with I-127 species for samples in the first 6 pore volumes (Figure 11c and d). Because the influent pore water had a low I-127 concentration (11 µg/L as iodate), effluent total I-127 showed an initial decrease, as the *in-situ* iodide leached from the sediment (first 2 pore volumes), then an increase as the injected iodate leached through the column (2 to 10 pore volumes). The separate iodide analysis (red diamonds in Figure 11c and d and expanded plots in Figure 12 12) clearly shows the iodide leaching from the sediment column along with essentially no iodate (blue triangles). The iodine-127 release rate was calculated at the 70 h stop flow event at 2 pore volumes (Table 14).

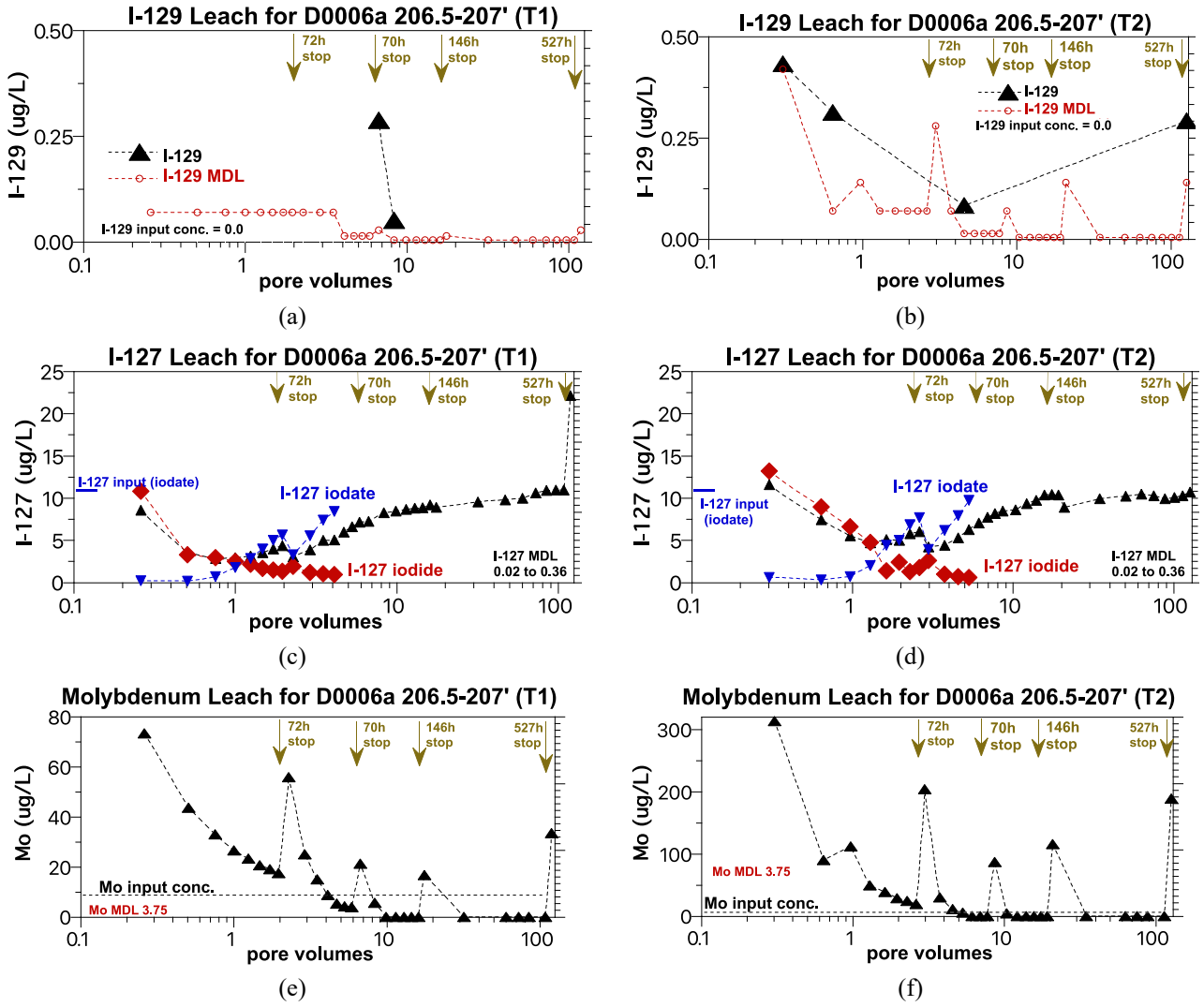

Figure 11. 1-D column leach results for D0006A, 206.5 to 107 ft depth sediment for experiments T1 and T2 (duplicate experiment) showing I-129 (a and b), I-127 (c and d), and Mo (e and f).

Although molybdenum (Mo) is not a contaminant of concern, it was necessary to quantify in effluent samples for total I-129 analysis. Initial molybdate (i.e., only aqueous species present, Figure 3b) in the effluent was 75 to 300 µg/L (Figure 11e and f), so significant sample dilution was required to reduce Mo to less than 2 µg/L for total I-129 analysis. Molybdate decreased to below detection limits by 10 pore volumes. The total leached Mo was 0.19 µg/g and 1.02 µg/g (Figure 11e and f), comparted to an estimated total extractable Mo in uncontaminated sediment of 0 to 2 µg/g (Table 11 footnote, DOE, 1993). This appears to be a significant fraction of mobile Mo, but there is little known about the natural or anthropogenic molybdate transport in sediments. If the Mo is from the stainless steel (which is approximately 2% Mo), there should be significant Fe, Cr, and Ni, all of which are present in much higher concentration in the steel, although they have different transport and precipitation properties. The Fe and Ni should generally precipitate, but Cr (as chromate) could remain mobile. Therefore, although Mo is leaching from the sediment, because little is known about natural Mo leaching and the inconsistency with other metals in the stainless steel, it is unlikely that the Mo is from the stainless steel.

At each stop flow event, there was a significant increase in the molybdate concentration, indicating nonequilibrium between surface and solution Mo phases and slow release of Mo from the sediment into pore water. Mechanisms could include diffusion of aqueous molybdate in immobile pore water (which should be relatively rapid and only within a few pore volumes), or dissolution of one or more solid phases releasing Mo into solution. Calculation of the Mo release rates at the four stop flow events show only a small decrease between 2 and 130 pore volumes (Table 14, Figure 13). This may indicate the same surface phase releasing molybdate, such as molybdate substitution in calcite. In contrast to these results, calculation of uranium and chromium release rates in sediments over a greater number of pore volumes generally shows an orders of magnitude decrease, as high solubility phases are initially releasing contaminants in the first few pore volumes, then a low solubility phase slowly releasing contaminants (at a slower rate) at a large number of pore volumes.

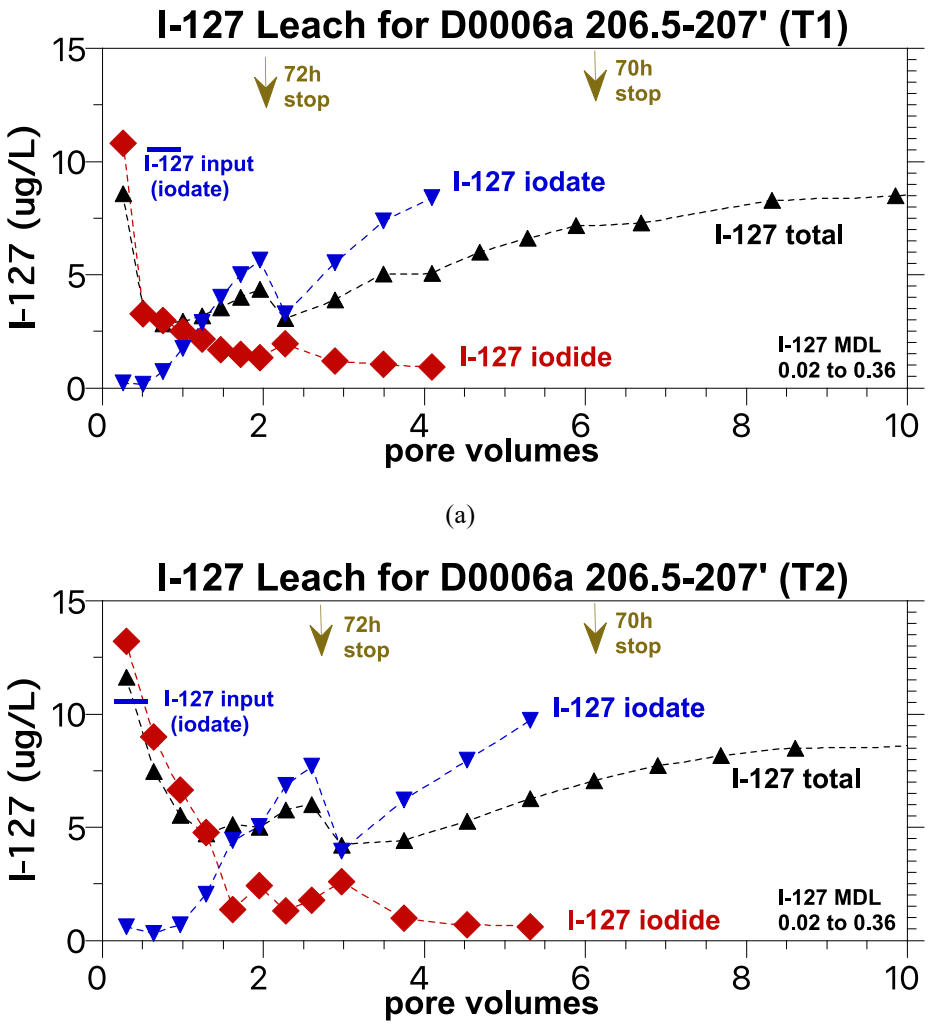

Figure 12. 1-D column leach results for D0006A, 206.5 to 207 ft depth showing the first 10 pore volumes of I-127 total, I-127-iodide, and I-127-iodate for experiments T1 (a) and T2 (b).

Table 14. Molybdenum and I-127 iodide release rates from sediment calculated from stop flows.

PNNL #	Borehole	Depth (ft)	HEIS #	COC	Release Rate at 2 pv (µg/Kg/day)	Release Rate at 7 pv (µg/Kg/day)	Release Rate at 18 pv (µg/Kg/day)	Release Rate at 110 pv (µg/Kg/day)
T1	D0006A	206.5-207	B3TF37	Mo	3.62	1.70	0.78	1.56
T2	D0006A	206.5-207	B3TF37	Mo	15.1	7.39	4.70	7.65
T1	D0006A	206.5-207	B3TF37	I-127 iodide	0.057			
T2	D0006A	206.5-207	B3TF37	I-127 iodide	0.067			

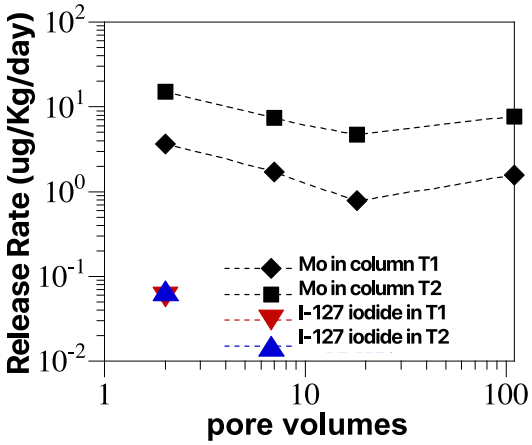

Figure 13. Change in the molybdenum and I-127 release rate over time during leach experiments.

4.3.2 Iron and Manganese Extractions

Iron (Fe) and manganese (Mn) extractions were conducted to characterize the potential for contaminant reduction in the sediments. The relative distribution of Fe and Mn in different forms provides insight into the sorptive and reactive capacity of the sediments. Table 15 and Table 16 show the results of the extractions and Fe and Mn analyses. For context, Fe is also plotted, showing the relative portions of different Fe(II/III) forms and the relative amounts of redox-active iron and ferrous iron phases (Figure 14a) and Mn phases (Figure 14c). The D0006A 106.5 to 107 ft depth sediment contained a total of 15.8 mg/g extractable iron (ferrous and ferric), based on a 3-week extraction in 5 M HCl. This Hanford formation (H2) sediment contains a mixture of mafic (i.e., sediments derived from basalt) and granitic minerals, with mafic minerals (pyroxenes, amphiboles) and clay minerals containing significant Fe and Mn phases. Ferrous phases were a small (2.5 mg/g) fraction of the total iron. There was no measurable adsorbed ferrous iron and the siderite/iron sulfide mass was also small (< 0.46 mg/g), so the environment was predominantly oxic, as the total ferrous phases were ~15% of the total iron. For ferric phases, the amorphous and crystalline iron oxides were also small (< 2.2 mg/g; available for microbial Fe reduction), whereas most of the ferric iron was likely in pyroxene and amphibole phases. Although all of these sediments are from the vadose zone, if water saturated, some abiotic reduction does occur (Szecsody et al. 2014) due to the small mass of ferrous iron from carbonates/sulfides. The ratio of ferrous and ferric iron and the total Fe in this sediment was comparable to other vadose zone sediments at Hanford (Figure 14b) in both the Hanford and Ringold formations.

Although the total Mn(II) and Mn(IV) extracted from the sediment (0.29 mg/g, Table 16) was 1% to 2% of the total iron in the sediment, there was a greater fraction of potentially redox reactive Mn(II) phases (purple in Figure 14c). The amount of ion exchangeable Mn(II) was small (0.001 mg/g), but the Mn(II) associated with carbonates (0.13 mg/g) was significant. Mn(II) phases were ~30% of the total Mn.

Table 15. Iron extraction results.

Borehole, depth (ft)	HEIS #	Ads. Fe^{II} (mg/g)	$Fe^{II}CO_3$, FeS (mg/g)	Other Fe^{II} (mg/g)	Am. Fe^{III} (mg/g)	Crys. Fe^{III} (mg/g)	Other Fe^{III} (mg/g)	Total Fe^{III} (mg/g)
D0006A, 206.5-207	B3TF37	< 0.005	0.46	2.01	0.067	2.16	13.8	16.0
D0006A, 206.5-207 dup	B3TF37	< 0.005	0.36	--	0.057	2.04	13.5	15.6

Table 16. Manganese extraction results.

Borehole, depth (ft)	HEIS #	Ads. Mn^{II} (mg/g)	$Mn^{II}CO_3$ (mg/g)	Am. Mn^{II+IV} (mg/g)	Crys. Mn^{II+IV} (mg/g)	Total Mn^{II+IV} (mg/g)
D0006A, 206.5-207	B3TF37	0.00056	0.127	0.098	0.088	0.300
D0006A, 206.5-207 dup	B3TF37	0.00202	0.134	0.090	0.093	0.279

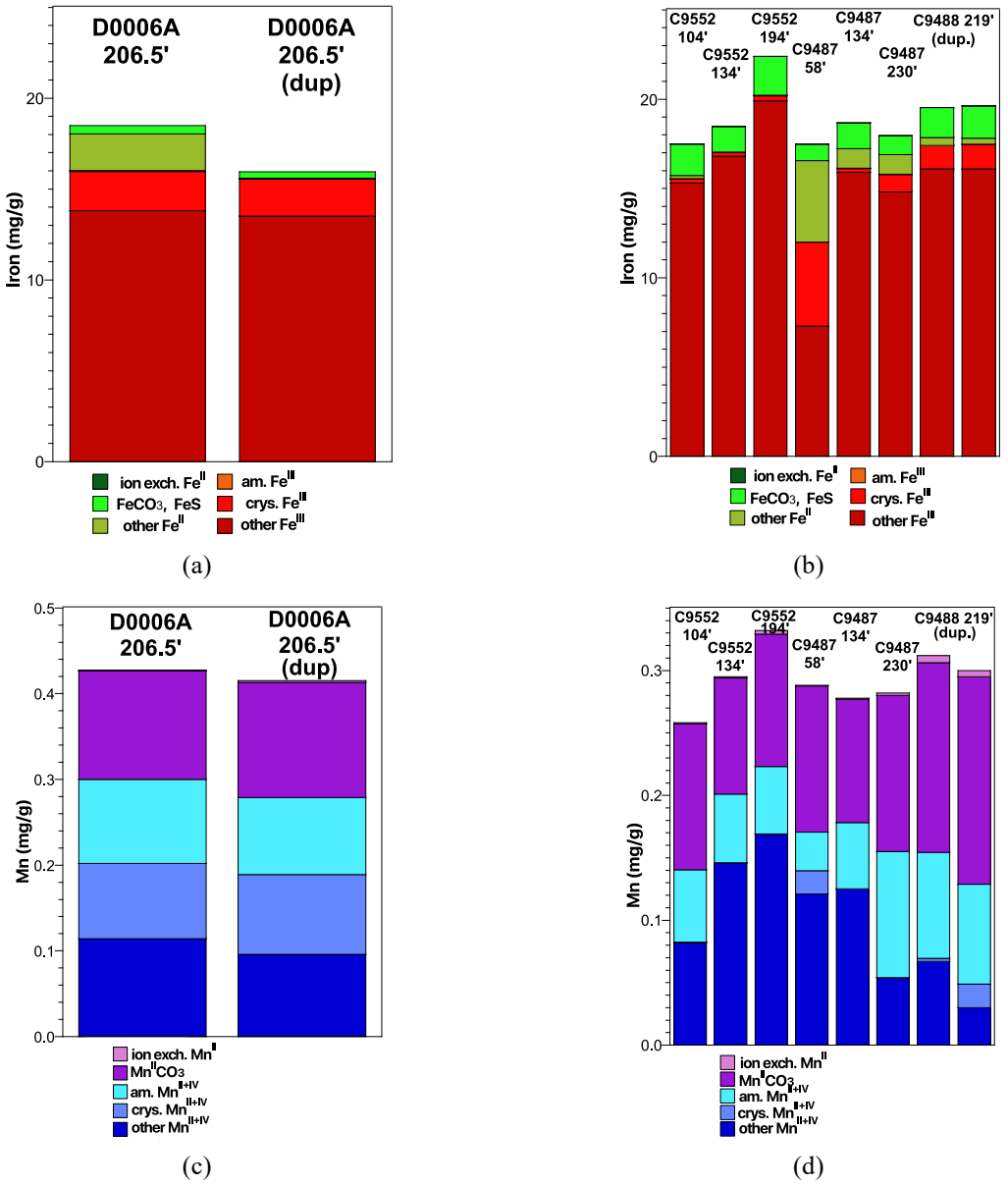

Figure 14. Iron extraction results for D0006A, 206.5 to 207 ft depth (a), a comparison to other B-complex vadose zone iron extractions (b), manganese extraction results for D0006A, 206.5 to 207 ft depth (c), and a comparison to other B-complex vadose zone manganese extractions (d).

5.0 Conclusions

This study was initiated to characterize subsurface contaminants in the A-AX vadose zone (principle study question, PSQ #2), distribution of contaminants in pore water and solid phases (PSQ #4), sediment phases that may be altered by contaminants, and estimate chemical and physical properties of sediments that influence contaminant movement. Possible sources are waste releases from nearby tanks, chemical processes, and disposal ditches, including a) A-104 and/or A-105, b) 242A evaporator, and c) 200-E-286 ditch. Additional elements were also analyzed to determine if the waste releases resulted in corrosion of the stainless-steel casing of wells. A tiered approach was used for characterizing contaminants in samples from boreholes D0006 and D0008, which includes:

- Tier 1: estimate mobile and total contaminant concentrations and sediment physical properties,
- Tier 2: characterize contaminant speciation as an indicator of contaminant movement potential, and
- Tier 3: measure contaminant leaching to quantify the mass and release rates from sediments

Contaminant concentration screening (Tier 1) of seven depths in both boreholes showed elevated sulfate and nitrate in all samples (130 to 280 ft depth), elevated chloride in five depths, and no elevated radionuclides except I-129 in D0006 at 206 to 208 ft depth. The elevated nitrate, sulfate, and chloride indicate waste could initially have been acidic (i.e., sulfuric, nitric, hydrochloric acid), which would lead to stainless steel corrosion. An acidic spill near surface would have been neutralized within tens of feet of depth in the vadose zone given the moderate to high acid neutralization capacity of the sediment, so stainless-steel casing corrosion would have been more likely in shallow sediments. However, current elevated chloride concentrations (pH neutral) at depth are sufficiently high result in some corrosion of stainless-steel surface, especially at welds. GEL labs data also shows low (but above natural) chromate from shallow to 170 ft depth, then higher chromate to 280 ft, which suggests chromate leaching from a surface spill or casing dissolution. GEL labs data also showed evidence of more than one plume, as nitrate, pertechnetate, and iodide (iodide or iodate) was found at depth (> 130 ft), but tritium, which is also a highly mobile contaminant, was found in shallow sediment (20 to 80 ft). Disposal from the 200-E-286 ditch from 1946 to 1953 in combination with tank leaks, then a later 60,000-gallon water line leak in 1978 could have resulted in the multiple infiltrating plumes. Elevated aqueous cations and anions in the D0006 at 206 to 208' depth pore water (SO_4^{2-}, NO_3^-, Na^+, K^+, Ca^{2+}, Mg^{2+}, Si) could be the result of acid disposal and calcite dissolution at shallow, with deeper migration of SO_4^{2-}, NO_3^- from acids and Ca^{2+} and $Mg^{2+}$from calcite. Elevated Si (160 mg/L) indicates dissolution of clays or other silicates, which can also occur in acids. Although there is no direct indication of acids reacting with sediments because sediments from 130 to 280 ft depth have near natural pH (7.6 to 7.9) and 1.65% calcite. In contrast, acid disposal at other sites at Hanford (300A, U-8 crib) showed depeleted calcite in shallow sediments. Acid extractable metals do show elevated Cr but not Fe, Ni, Mo, and Mn above natural levels (metals present in 304L and 316L stainless steel), so may be an indication of stainless steel well corrosion or transport of Cr from a shallow spill (i.e., 200-E-386 ditch), if an acid spill were leaching through the vadose zone.

Additional I-129 speciation (Tier 2) and transport (Tier 3) analysis was conducted on the D0006 206 to 208 ft depth sample. The total I-129 in aqueous extractions (0.00034 mg/g) was 23% of the total I-129 in the sediment (0.0015 mg/g), as defined by the tetramethylammonium hydroxide (TMAH) extraction. Although the total I-129 and I-129 species was below detection limits in most extraction samples due to high molybdate, I-127 analysis provided some insight into possible I-129 surface phases. Total I-127 in sequential acidic extractions (0.15 mg/g) showed I-127 as 23% aqueous and adsorbed (highly mobile) and in precipitates dissolved with pH 5 acetate (21%), pH 2.3 acetic acid (46%, likely calcite), and 10% in hard to extract phases. Nearly all the I-127 was present as iodide. The I-127/I-129 in the A-AX tanks of 1 to 7 were diluted in pore water at this depth to 45 to 63. Because a significant amount of I-127 was present associated with calcite, the 1000-h carbonate extraction showed that a significant amount of I-127 (0.075 mg/g) is potentially mobile. The TMAH extraction showed additional I-127 was present in

alkaline precipitates (TMAH extraction 0.276 mg/g). I-127 was likely not associated with organic matter, as the total organic carbon (TOC) in pore water and in sediment was below detection limits (< 0.005%). The total inorganic carbon measurement of the sediment identified 1.65% calcite. It is possible that iodine was incorporated into calcite based on its presence in the acetic acid and carbonate extractions as well as a previous study that has shown that iodine can be incorporated into calcite.

Iodine 1-D column leach experiments (Tier 3 analysis) were conducted to measure mobility of iodine with analysis of total I-129, total I-127, associated I-127 and I-129 species, and molybdate, which was needed for I-129 measurements. There was little direct information on I-129 leaching as only a few samples could be measured for total I-129 due to interference by molybdate. However, the I-127 leached from the sediment within 2 pore volumes was present entirely as iodide and was much smaller than predicted from sequential extractions or the 1000-h carbonate extraction. The I-127 release rate calculated at a stop flow event was 0.06 mg Kg^{-1} day^{-1}. Molybdenum, also measured in the 1-D column leach experiments, present as molybdate, was dynamic, with a high initial concentration (300 µg/L) which decreased to below detection limits by 10 to 130 pore volumes. But, at each of the four stop flow events from 2 to 130 pore volumes, there was a large molybdate increase. The calculated Mo release rates from sediment did not decrease with increasing pore volumes, which suggested Mo was being released from the same precipitate phase, such as molybdate incorporated into calcite. The source of Mo was most likely natural sources based on the absence of co-contaminants (Fe, Ni, Cr) which are present at higher concentrations in stainless steel that would indicate well corrosion.

Overall, because there was little radioactive contamination measured in D0006 and D0008 boreholes other than I-129 at the 206 to 208 ft depth in D0006, contaminants potentially released from A-104 and A-105 did not reach this location south of the A tank farm. Elevated cations and anions found at depth could be the result of acidic disposal that could cause shallow stainless steel casing corrosion or could be the result of infiltration of acidic water reacting with sediment. The nearby 242A evaporator contained alkaline waste (and tritium), but the nearby 200-E-286 ditch generally contained liquid effluent with high chloride. Stainless steel component metals were generally not elevated at the 206 to 208 ft depth except for Cr, which could be from casing corrosion and the high mobility of Cr as chromate or Cr surface disposal. The depth profiles of contaminants (sulfate 130 to 210 ft depth, chromate 180 to 280 ft depth, nitrate 130 to 220 ft depth, chloride 130 to 210 ft depth, tritium 20 to 80 ft depth) suggests at least two plumes to account for mobile contaminants at depth (i.e., chromate, nitrate, chloride) as well as a highly mobile contaminant in shallow sediment (tritium).

6.0 Quality Assurance

This work was performed in accordance with the Pacific Northwest National Laboratory Nuclear Quality Assurance Program (NQAP). The NQAP complies with DOE Order 414.1D, *Quality Assurance*. The NQAP uses NQA-1-2012, *Quality Assurance Requirements for Nuclear Facility Application* as its consensus standard and NQA-1-2012 Subpart 4.2.1 as the basis for its graded approach to quality.

7.0 References

Beckett, P. 1989. The use of extractants in studies on trace metals in soils, sewage sludges, and sludge-treated soils. In Advances in Soil Science, Volume 9, Springer-Verlag, New York, p 144-176.

Brina, R. and A.G. Miller. 1992. Direct detection of trace levels of uranium by laser induced kinetic phosphorimetry. Analytical Chemistry 64(13):1413-1418.

Chao, T. and L. Zhou. 1983. Extraction techniques for selective dissolution of amorphous iron oxides from soils and sediments. Soil Science Society of America Journal 47(2):225-232.

DOE. 1993. *Hanford Site Background: Part 1, Soil background for nonradioactive analytes*. DOE/RL-92-94 Revision 1, UC-630, 721, p 243.U.S. Department of Energy, Richland, Washington.

Garcia, C., M. de Tiedra, Y. Blanco, O. Martin, and F. Martin. 2008. Intergranular corrosion of welded joints of austenitic stainless steels studied by using an electrochemical minicell. Corrosion Science, 50, 2390-2397.

Gibbs, C. 1976. Characterization and application of ferrozine iron reagent as a ferrous iron indicator. Analytical Chemistry 48(8):1197-1200.

Gleyzes, C., S. Tellier, and M. Astruc. 2002. Fractionation studies of trace elements in contaminated soils and sediments: a review of sequential extraction procedures. Trends in Analytical Chemistry 21(6 & 7):451-467.

He, W., O. Knudsen, and S. Diplas. 2009. Corrosion of stainless steel 316L in simulated formation water environment with CO2-H2S-Cl-. Corrosion Science, 51, 2811-2819.

Heron, G., Crouzet, C., Bourg, A.C. and Christensen, T.H., 1994b. Speciation of Fe(II) and Fe(III) in contaminated aquifer sediments using chemical extraction techniques. Environmental Science and Technology, 28: 1698-1705.

Kimmig, S., Thompson, C., Baum, S., and C. Brown. 2021. Evaluation of iodine speciation oand 129-I/127-I ratio at low concentrations in environmental samples using IC-ICP-MS. J. Radioanalytical and Nuclear Chemistry, 327, 929-937.

Klages, D., Holm, M., and D. Parker, 2021. Waste Management Area Integration Study - Waste Management Area A-AX, RPP-PLAN-64407 Rev 0, Washington River Protection Solutions, Richland, Washington.

Kohler, M., D.P. Curtis, D.E. Meece, and J.A. Davis. 2004. Methods for estimating adsorbed uranium (VI) and distribution coefficients of contaminated sediments. Environmental Science and Technology 38:240-247.

Larner, B., A. Seen, and A. Townsend. 2006. Comparative study of optimized BCR sequential extraction scheme and acid leaching of elements in certified reference material NIST 2711. Analytica Chimica Acta 556:444-449.

Lawter, A., Garcia, W., Kukkadapu, R., Qafoku, O., Bowden, M., Saslow, S., and N. Qafoku. 2018. Technetium and iodine aqueous species immobilization and transformations inthe presence of strong

reductants and calcite-forming solutions: Remedial action implications. Science of the Total Environment, 636, 588-595.

Lee, B., Szecsody, J. Qafoku, N., McElroy, E., Baum, S., Snyder, M., Lawter, A., Resch, C., Gartman, B., Zhong, L., Saunders, B., Williams, B., Horner, J., Leavy, I., Christiansen, B., Clayton, R., and K. Johnson, 2017, Contaminant attenuation and transport characterization of 200-UP-1 Operable Unit sediment samples. Pacific Northwest National Laboratory, Richland, WA, PNNL-26984.

Li, L., C. Dong, K. Xiao, J. Yao, and X. Li. 2014. Effect of pH on pitting corrosion of stainless steel welds in alkaline salt water. Construction and Building Materials. 709-715.

Marcus, P., 1998. Surface science approach of corrosion phenomena. Electrochimica Acta, 43(1-2), 109-118.

Martin, F., P. Matishan. E. Lemieux, T. Newbauer, R. Rayne, R. Bayless, H. Kahn, G. Michal, F. Ernst, and A. Heuer. 2009. Enhanced corrosion resistance of stainless steel carburized at low temperature. Metallurgical and Materials Transactions A, vol 40A, 1805-1811.

Mossop, K. and C. Davison. 2003. Comparison of original and modified BCR sequential extraction procedures for the fractionation of copper, iron, lead, manganese, and zinc in soils and sediments. Analytica Chimica Acta 478:111-118.
McNally, S., 2011. The status of iodine and selenium in Waikato soils. University of Waikato, Hamilton, New Zealand, M.S. thesis. https://hdl.handle.net/10289/5375

Reynolds, J., 2021. The isotopic composition of iodine in Hanford radioactive tank waste, Waste Management, March 8-12, 2021, 21144.

Rhoades, J.D. 1996. Methods of soil analysis, Part 3. Chemical Methods. Madison, Wisconsin, Soil Science Society of America.

Robertson, J., 1991. The mechanism of high temperature aqueous corrosion of stainless steels. Corrosion Science, 32(4), 443-465.

Routson, R., G. Barney, R. Smith, C. Delegard, and L. Jensen. 1981. Fission product sorption parameters for Hanford 200 area sediment types. Rockwell International, Richland, WA, RHO-ST-35

RPP-RPT-60227, Tabor, C., and K. Schuyler, 2020, Data Quality Objectives for Vadose Zone Characterization at Waste Management Area A-AX, Rev. 1, Washington River Protection Solutions, Richland, Washington.

Sedricks, A., 1996. Corrosion of Stainless Steel. John Wiley & Sons, Inc., New York, New York.

Sutherland, R. and F. Tack. 2002. Determination of Al, Cu, Fe, Mn, Pb, and Zn in certified reference materials using the optimized BCR sequential extraction procedure. Analytica Chimica Acta 454:249-257.

Szecsody, J.E., H.P. Emerson, C.I. Pearce, C.T. Resch and S.A. DiPietro. 2020b. In situ reductive dissolution to remove precipitated Iodine-129 from aquifer sediments. J. Env. Radioactivity, 216, 1-10.

Szecsody, J., C. Bagwell, R. Mackley, and S. Hoyle. 2020a. Evaluation of ammonia discharge into PUREX Crib 216-A-37-1 and nitrogen species fate in the subsurface. Pacific Northwest National Laboratory, PNNL-29999, Richland, WA.

Szecsody, J., M. Truex, N. Qafoku, J. McKinley, K. Ivarson, and S. Di Pietro. 2019. Persistence of chromate in vadose zone and aquifer sediments in Hanford, Washington, Science of the Total Environment, 676, 482-492.

Szecsody J.E., C.I. Pearce, K.J. Cantrell, N. Qafoku, G. Wang, E.C. Gillispie, and A.R. Lawter. 2018. Evaluation of Remediation Technologies for Iodine-129: FY18 Bench Scale Results. PNNL-28064. Richland, WA: Pacific Northwest National Laboratory.

Szecsody, J.E., Jansik, D., McKinley, J.P., and N. Hess, 2014, Influence of alkaline waste on technetium mobility in Hanford formation sediments. J. Environmental Radioactivity, 135, 147-160.

Szecsody, J., M. Truex, N. Qafoku, D. Wellman, T. Resch, and, L. Zhong, 2013, Influence of acidic and alkaline co-contaminants on uranium migration in vadose zone sediments. J. Contaminant Hydrology, 151, 155-175.

Szecsody, J., Truex, M., Lee, B., Strickland, C., Moran, J., Snyder, M., Resch, C., Zhong, L., Gartman, B., Saunders, D., Baum, S., Leavy, I., Horner, J., Williams, B., Christiansen, B., McElroy, E., Nims, M., Clayton, R., and D. Appriou, 2017, Geochemical, Microbial, and Physical characterization of 200-DV-1 Operable Unit B-Complex Cores from Boreholes C9552, C9487, and C9488 on the Hanford Site Central Plateau, Pacific Northwest National Laboratory, PNNL-26266.

Szecsody J.E., C.I. Pearce, K.J. Cantrell, N. Qafoku, G. Wang, E.C. Gillispie, and A.R. Lawter. 2018. Evaluation of Remediation Technologies for Iodine-129: FY18 Bench Scale Results. PNNL-28064. Richland, WA: Pacific Northwest National Laboratory.
Tabor, C., and K. Schuyler. 2019. Sampling and analysis plan for WMA A-AX focus area 2 (Southwestern area of A farm). Washington River Protection Solutions, RPP-PLAN-63020, Revision 0.

Tabor, C., 2021. WMA A-AX Vadose Zone Soil Investigation. Washington River Protection Solutions, TOC-PRES-21-1832-VA revision 0.

Truex, M., J. Szecsody, N. Qafoku, C. Strickland, J. Moran, B. Lee, M. Snyder, A. Lawter, C. Resch, B. Gartman, L. Zhong, M. Nims, D. Saunders, B. Williams, J. Horner, I. Leavy, S. Baum, B. Christiansen, R. Clayton, E. McElroy, D. Appriou, K. Tyrell, M. Striluk, 2017, Contaminant Attenuation and transport characterization of 200-DV-1 Operable unit sediment samples, Pacific Northwest National Laboratories, PNNL-26208.

Um, W., J. Serne, M. Truex, A. Ward, M. Valenta, C. Brown, C. Iovin, K. Geiszler, I. Kutnyakov, E. Clayton, H. Chang, S. Baum, R. Clayton, and D. Smith. 2009. Characterization of sediments from the soil desiccation pilot test (SDPT) site in the BC Cribs and Trenches area. Pacific Northwest National Laboratory, PNNL-18800, Richland, WA.

Watts, T., and E. Mitchell. 2008. A pilot study on iodine in soils of Greater Kabul and Nangarhar provinces of Afghanistan", Env. Geochem. Health 31(4).

Xie, Y, Murray, C., Last, G., and R. Mackley, 2003. Mineralogical and bulk-rock geochemical signatures of Ringold and Hanford formation sediments. Pacific Northwest National Laboratory, PNNL-14202, Richland, WA.

Zachara, J., C. Liu, C. Brown, S. Kelly, J. Christensen, J. McKinley, J. Davis, J. Serne, E. Dresel, and W. Um. 2007. A Site-Wide Perspective on Uranium Geochemistry at the Hanford Site. Pacific Northwest National Laboratory, Richland, Washington (PNNL-17031).

Zhang, S., Xu, C., Creeley, D., Ho, Y.-F., Li, H.-P., Grandbois, R., Schwehr, K.A., Kaplan, D.I., Yeager, C.M., Wellman, D., 2013. Iodine-129 and Iodine-127 speciation in groundwater at the Hanford site, US: iodate incorporation into calcite. Environ. Sci. Technol. 47 (17), 9635–9642.

Appendix A – Data from Boreholes D0006/6A and D0008/8A analyzed by GEL Laboratories

Table A.1. Radionuclide, metals, and anion data for borehole D0006.

sample	depth (ft)	Cs-137 (pCi/g)	I-129 (pCi/g)	Sr-90 (pCi/g)	Tc-99 (pCi/g)	H-3 (pCi/g)	U (ug/Kg)	F- (ug/Kg)	Cl- (ug/Kg)	NO3 (ug/Kg)	NO2 (ug/Kg)	SO4 (ug/Kg)	Cr(VI) (ug/Kg)	H2O (%)
B3TF91	0	0.14	0.0774	0.371	-0.53	-0.0524	456	351	8280	70400	1120	6650	106.	5.38
B3TF92	0	0.118	0.0045	-0.913	-0.949	0.0369	547	618	7210	69500	1150	6990	149.	5.37
B3TFB6	7	0.0702	-0.258	0.934	-1.63	0.32	536	1630	4790	9870	1220	4980	107.	9.98
B3TFB7	12	-0.0024	-0.0634	-1.	-1.74	3.85	600	2290	8130	8990	1190	10300	108.	7.96
B3TFB8	20	0.0391	0.198	-1.06	-1.83	18.1	513	1010	9150	7700	1130	6760	162.	6.55
B3TFB9	79	-0.0003	0	-0.598	0.0323	19.5	465	720	6740	8190	1140	10400	161.	4.85
B3TFC0	132	-0.0098	0.0916	-0.505	-2.13	1.67	502	869	17900	15300	1150	83800	156.	7.04
B3TFC1	179	0.0141	-0.0483	-0.795	2.28	1.87	619	555	11000	19500	1170	96400	167.	5.58
B3TFC2	204	-0.0046	0.202	0.51	5.25	0.308	732	692	19500	46500	1170	103000	579.	5.31
B3TFC3	260	0.244	-0.296	0.504	1.18	-1.78	496	917	6220	7390	1110	34300	3850.	2.39
B3TFC4	273	-0.0025	0.145	-0.828	0.714	-2	518	1010	13700	22800	1170	120000	2230.	7.24
MDL:		0.056	0.609	1.97	4.24	2.77	13.6	351	744	1510	1150	1430	169.	

Table A.2. Radionuclide and selected anion data for borehole D0008 from Gel

Quick Turn or Standard Analysis Results for D0008/A

Lithologic Unit	Depth (ft bgs)	Lab Performing Analysis	% H_2O	Nitrate (µg/g)	Sulfate (µg/g)	Tc-99 (pCi/g)	pH	Conductivity (µMHO/cm)
Backfill	Surface	GEL/222-S	4.21/2.76	1.47(U)/12.4	2.5(B)/5.01	-1.57(UX[a])/ 0.0606(U)	8.85(X[c])/8.45	N/A/136
H1	9-11	GEL/222-S	7.66/12.6	8.72/8.70	6.03/5.03	-0.890(UX[b])/ 0.0616(U)	9.36(X[c])/8.89	N/A/279
	12-14	GEL/222-S	1.98/2.93	3.06(B)/2.55	4.12/5.07	-0.607(UX[b])/ 0.0609(U)	9.93(X[c])/9.71	N/A/249
	22-24	222-S	6.46	3.70	19.9	0.0607(U)	8.90	217
	69-71	222-S	4.65	2.21	13.0	0.0609(U)	8.62	174
	130-132	222-S	2.95	3.01	27.7	0.0607(U)	8.79	219
H2	187-189	222-S	3.24	6.65	41.3	0.0607(U)	8.63	248
	262-264	222-S	4.63	14.6	72.4	0.104(JX)	8.02	337
CCu(silt)	276-278	222-S	29.1	56.1	348	0.0802(JX)	7.79	925
CCu(gravel)	282-284	222-S	5.79	7.93	82.9	0.0609(UX)	8.28	318

Note:
GEL does not perform water digest for "quick turn" analysis the way 222-S does and therefore performed extractions per method procedure (standard analysis). 222-S performs "quick turn" analysis using 1:1 water digest method, as described in SAP Table 4-3, footnote "k".
B – Analyte detected in both the sample and the associated blank.
N/A – not available.
U – Result is less than the Detection Limit.
X – GEL qualifiers
a. Did not meet the resolution requirement for the tracer
b. Reprepped due to low carrier/tracer yield. The re-analysis is being reported.
c. The analysis was performed outside the hold time.
bgs – below ground surface

Pacific Northwest National Laboratory

902 Battelle Boulevard
P.O. Box 999
Richland, WA 99354
1-888-375-PNNL (7665)

www.pnnl.gov